4 Radiation budget of the climate system

This chapter summarizes a few basic facts on the role of radiant energy in maintaining our present climate. It concentrates in particular on a rather complete data set of global maps and of related statistics on the radiation budget components at both boundaries of the atmosphere, on the vertical columnar divergence or convergence of radiant energy and on the possible effect of clouds on these quantities. We have chosen here a unique data set, which has been computed within the frame of the International Satellite Cloud Climatology Project ISCCP (99Ros). Also the information on clouds, as it is discussed in chapter 5 of this volume by C. Stubenrauch, is derived from the same satellite measurements. Maps of other energy fluxes at the surface, shown in chapter 10 of this volume, complement this data set.

This ISCCP data set covers now a period of more than 19 years, beginning in 1983. We selected the period of the complete years **1991 to 1995** to provide maximum overlap with the other geophysical data discussed in this volume. This data set has been calculated from cloud and other information on the state of the climate system within the International Satellite Cloud Climatology Project (ISCCP; 99Ros). It is not identical with specifically dedicated measurements of the earth's radiation budget at the top of the atmosphere (TOA) from satellites since the year 1960 (e.g. 72Ras, 95Wie, 02Wie). Such other measurements have frequently been done in the past, but mostly over shorter time periods and only from a single polar orbiting satellite, while the ISCCP data is obtained from at least two polar and 3 to 4 geostationary satellites, to improve temporal sampling over areas of rapid changes. Only recently the dedicated radiation budget measurements became operational onboard of at least two polar orbiters and on the new European geo-stationary satellite MSG (Meteosat Second Generation), thus reducing the spectral and temporal sampling errors.

We further add in the last sections of this chapter 4 some details on the PAR (**P**hotosynthetically **A**ctive solar **R**adiation), on the UV-B dosage at ground, and on the radiative transfer properties of snow fields and of water (oceans). These latter quantities enable estimates of the effect of radiation on biomass production on continents and in the ocean, and of the radiative heating in upper snow and ocean layers on the basis of quite realistic information on the radiation budget at their surface, which in part can be estimated from the same ISCCP radiance data sets. A few other aspects of the radiation budget at ground are discussed in section 10 of this volume.

Many scientists contributed to this compilation. The authors thank in particular Drs. W.B. Rossow and Y.-C. Zhang from the NASA Goddard Institute for Space Studies in New York for their special efforts to provide us their results and more details. Dr. M. Wild of the ETH Zürich gave us his comparisons of retrieved and measured downward long- and shortwave fluxes. Dr. R. Pinker of the University of Maryland provided her results on the Photosynthetically Active Radiation (PAR) and Dr. M. Madronich of the NCAR, Boulder Colo., made his data on the near surface UV-B radiation available for this publication. Drs. J. Lean and C. Froehlich gave us their recent results on the solar constant. We also thank Drs. T.C. Grenfell (CRREL, Hanover), M. Kuhn (U. Innsbruck, Austria), W. Simpson (U. Fairbanks, Alaska), R. Hollmann, J. Meywerk and R. Doerffer (GKSS, Geesthacht), S. Warren (U. Washington, Seattle) and T. Yamanouchi (NIPR, Tokyo) for their information on the radiation properties of snow, water and ice, respectively. Mg. M. Kottek of the University for Veterinary Medicine in Vienna, Austria, created with greatest care and patience all maps and most other figures from the above-mentioned data sets. This work began while E.R. was visiting professor at the Center of Climate System Research of the University of Tokyo, where deep discussions helped considerably.

The list of references in chapter 4.6 is by far not complete; but it should allow to inform on deeper details.

4.1 Introduction and conventions

All processes in the climate systems of the Earth and of the other terrestrial planets Mercury, Mars and Venus are in principle forced by the exchange of energy by electromagnetic radiation between space (here: the Sun) and these planets at various wavelength intervals. The Sun is the only energy source, since the heat transfer from the interiors of these planets is at least 5 to 6 orders of magnitude smaller than the solar irradiance reaching those planets. The subsequent solar heating produces thermal radiation (e.g.: 92Pei). Vertical and horizontal gradients of the net heating are the cause of complex circulation systems in the atmospheres and on earth and within the oceans. They are re-distributing heat from excess areas to deficit areas and are the intimate source of the climate. Life on earth is benefiting additionally from the presence of substantial amounts of water and stratospheric ozone (see section on Atmospheric water vapor).

In Fig. 4.1.1 are summarized all radiation quantities, which will be described in this chapter. They are the budgets and their individual components, and the cloud effects on them at the top and bottom (ground) of the atmosphere. Also the differences between these budgets are computed to illustrate the amounts of radiant energy either remaining in the atmosphere or lost to space. We count all downward fluxes as "positive" and all upward fluxes as "negative". Positive values of the vertical divergence mean then formally a "convergence" of radiant energy in the atmosphere, leading to its heating. On the other side, then negative values of the divergence describe a net loss of radiant energy, cooling the atmosphere to space.

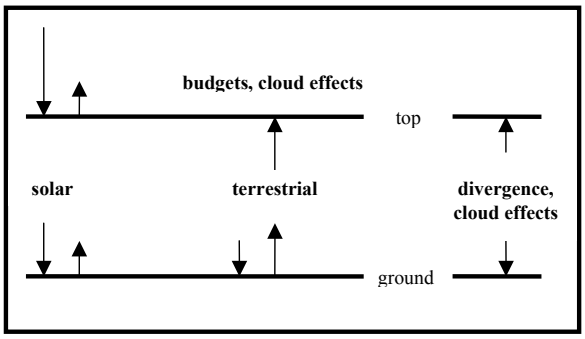

Fig. 4.1.1 This study describes the budgets of radiant energy, their vertical divergence and the clouds effects on them, which are calculated from the ISCCP radiance data sets. Since the Earth is heated only by the Sun, all **downward** radiation fluxes are counted **positive** and all **upward** fluxes are counted **negative**. Thus, a negative net flux density at the ground means loss of radiant energy into the atmosphere, etc. The vertical radiation "divergence" is the difference between net flux at the top (TOA) and at ground. In contrast to formal mathematics positive values mean here a convergence or gain of energy while negative values mean a divergence or loss of radiant energy in an atmospheric column.

On Earth, as shown schematically in Fig. 4.1.2**,** the major spectral ranges of interest of the incident solar radiation and of the terrestrial heat radiation are located within the spectral ranges between 0.2 and 4 μm and 4 and 100 μm (1 μm corresponds to 10^{-6} m), respectively, which overlap with only low power levels at 4 μm. Therefore we can formally distinguish between two components of the radiant energy flux: they are named according to their origin "**solar**" and "**terrestrial**" where the latter originates from the atmosphere and from the Earth's surface. They are often also quoted as shortwave and longwave components of radiant energy transfer. The spectral region between 0.4 and 0.7 μm is important for interactions with the vegetation. Therefore it is named "Photosynthetically Active Radiation (PAR)". This energy source for the biosphere can be estimated from the fields of downward solar radiation reaching the ground (95Fro). The UV-B component of solar radiation is located at wavelengths between 0.28 and 0.32 μm.

The Sun occurs as a heat source with an emission temperature of about 6000 K. However, only a small fraction of this enormous heat radiation reaches the Earth. This influx amounts to an annual average of slightly less than 342 Wm^{-2}, which is 1/4 of the solar irradiance (see section 4.3.2). The outgoing terrestrial heat radiation corresponds to an emission temperature of about 255 K. In absence of other significant internal heat sources, the earth should in global averages over at least one complete year be considered in radiative equilibrium with space.

The other two panels in Fig. 4.1.2 illustrate the spectral transparency of the cloudless atmosphere for downward radiation at ground and at an altitude of about 11 km. Numerous absorption bands and lines by oxygen, ozone, water vapor, carbon dioxide, methane and nitrous oxide (and other minor constituents) absorb effectively the short wave UV and the thermal infrared radiation in the atmosphere.

In numerical treatments of the atmospheric dynamics these radiation fluxes must be simulated with highest possible accuracy in any numerical circulation model. The entire diabatic heating of an atmospheric volume element is described by basic heat equations (see chapters by Hantel and by Hense in this volume).

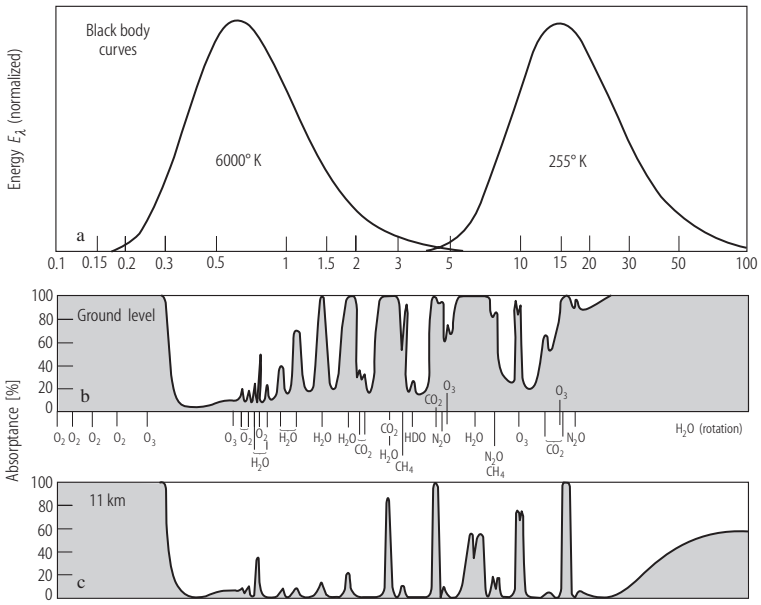

Fig. 4.1.2 Schematic spectra of downward solar radiation and of terrestrial radiation at the top of the atmosphere (panel a) and of the absorptance of the atmosphere as seen from ground (panel b) and at about 11 km altitude (panel c) for downward radiation (from (95Goo)). The abscissa describes the wavelength in μm. More details on the spectra are given e.g. in (86Sch) or in (99Tho).

4.2 Radiative transfer in the atmosphere

4.2.1 A few basic facts of radiative transfer in continua

Based on some international agreements on nomenclature in describing the transfer of radiation one has to distinguish between **radiances *L*** (radiation "beam" into a particular direction, given in units of aerial power density per angular element: $Wm^{-2}sr^{-1}$) and their integral over a particular plane (usually horizontal) surface, the **radiation flux density or irradiance *E*** or ***M*,** given in units of aerial power density Wm^{-2}. Further conventions to be observed are listed in the literature (e.g. 74Kas). These two quantities are primarily used in the text below. This introduction can only briefly summarize the involved areas. For more detail we refer to some recent textbooks: e.g. (95Goo), (92Lio), (92Pei), (86Sch), (98Sei); (99Tho). There are several basic laws applicable and well documented applying to radiative transfer in atmospheres. These are for heat radiation**:** Planck's law and the Stefan-Boltzmann law. For deriving a principle differential equation of radiative transfer we further can assume local thermodynamic equilibrium in almost all layers of the atmosphere below about 50 km, where the Kirchhoff law holds, that the absorption of radiant energy equals the emission.

The final differential equation of radiative transfer in an atmosphere considers sources (the Sun and scattered solar and emitted thermal radiation incident into a volume element and emitted within it, respectively) and sinks (scattering and transmitting out of a volume element into a particular direction). Its formal solution for the radiance L emerging from a volume element into directions δ and φ is shown below. The symbol J represents all sources. In an arbitrary coordinate system s is a geometric line, ρ is the density of air, k is the spectral extinction coefficient. All quantities refer to a particular wavelength.

$$L(\delta, \varphi) = L_0(\delta, \varphi)\, e^{-k\rho s} + \int J(s')\, e^{-k\rho s'}\, ds'$$

On Earth, the contribution of the Sun to the source term by solar radiation begins to become almost unimportant at wavelengths λ larger than about 5 μm, as shown in Fig. 4.1.2. There have been developed also solutions for various other geometries and applications, inclusive three-dimensional objects, such as fields of finite clouds. These include also the use of the technique to simulate neural networks (e.g. 01Goe).

During the past 4 to 5 decades a large variety of solutions for the differential equation has been developed with increasing spectral detail and complexity as the computational resources of the users become more and more powerful. Most sophisticated applications, such as for the interpretation of spectrally very high resolved satellite measurements can make use of information from data banks on the spectral absorption characteristics of each gas in the atmosphere (see section 4.2.4), while the extremely often repeated applications, as in models for the dynamics of the atmosphere-ocean system, must still make use of various simplifications. These cause systematic uncertainties.

4.2.2 Radiatively active components in the climate system

In the Earth's atmosphere the main gases O_2 and N_2 and also the noble gases participate only passively at wavelengths > 0.25 μm in scattering processes and in changes of the index of refraction. Oxygen is almost completely absorbing the incident solar radiation at wavelengths shorter than about 0.2 μm. However many other gases with often very small concentration can alter the radiation fields very effective, as shown already in Fig. 4.1.1, above. Such trace gases are the **water vapor**, **carbon dioxide**, **methane, and ozone**, **nitrous oxide** and the large variety of **CFCs** and other gases. Most of them are listed in Table 4.2.2.1 (from IPCC 2001).

These gases are responsible for the atmospheric greenhouse effect (see Section 4.2.5), where water vapor may already account for about 50 to 60 percent. Values of their abundance are given in various textbooks and reports and to some extent also in IPCC 2001. The increase of their concentration, which has been measured during the past 40 to 60 years, and the simultaneous present decrease of stratospheric ozone are assumed to provide an additional force in the atmosphere, which may alter our climate into an undesired direction (additional greenhouse effect).

4.2.3 Absorption and scattering in the clear and turbid atmosphere

Once the amount of particles in a volume element becomes larger than a critical value and once also the index of refraction of the particle deviates from that of the ambient gaseous atmosphere, then additional scattering processes occur, which however can be reduced by strong absorption in the medium. The same holds also for density fluctuations in water or in the air. Their numerical treatment provides also difficulties in related simulations.

Such scattering processes enlarge the pathlength of each light parcel or of photons and consequently increase the absorption of radiative energy in a medium. The angular dependence of the scattering is determined by the ratio of the size of a scatterer (either a particle or turbulent changes of the density in a gas but also in water) to the wavelength of light and the difference between the (complex) index of refraction of the scattering sources and the ambient medium of it, e.g. the gaseous atmosphere. Since a long time we use the laws for the "Rayleigh" scattering for scattering sources, which are about 3-4 orders of magnitude smaller than the wavelength of radiation. It also causes a strong polarization of the scattered radiation component. Here the scattering efficiency is proportional to the inverse fourth power of the wavelength.

When particles become larger with respect to the wavelength, the angular dependence becomes very complex showing usually a very high scattering efficiency into the forward direction, which is often several orders of magnitude larger than the sideward and backward scattering. The surface roughness may cause additional effects, which in particular need to be taken into account in remote sensing applications. Earlier parameterizations made use of the well-known "Mie-Theory", which assumed spherical dielectric particles. Now other shapes and also other dielectric properties can be treated. Here the scattering efficiency is approximately proportional to the 1.3-th inverse power of the wavelength.

Table 4.2.2.1 Summary of atmospheric greenhouse gases, which are also subject to originate in part from anthropogenic activities, (from IPCC 2001, Technical Summary). The major greenhouse gas, **water vapor, which is not listed here**, contributes about 50 to 60 % of the total greenhouse effect. Also the ozone in the stratosphere and at ground contributes significantly to the atmospheric greenhouse effect. "The Global Warming Potential" relates the emission of 1 kg of each gas to emission of 1 kg carbon dioxide. The calculations for different time horizons show the effects of lifetimes of each gas.

Gas		Lifetime (years)	Global Warming Potential (Time Horizon in years)		
			20 yrs	100 yrs	500 yrs
Carbon dioxide	CO_2		1	1	1
Methane[a]	CH_4	12.0[b]	62	23	7
Nitrous oxide	N_2O	114[b]	275	296	156
Hydrofluorocarbons					
HFC-23	CHF_3	260	9400	12000	10000
HFC-32	CH_2F_2	5.0	1800	550	170
HFC-41	CH_3F	2.6	330	97	30
HFC-125	$CHF_2\,CF_3$	29	5900	3400	1100
HFC-134	CHF_2CHF_2	9.6	3200	1100	330
HFC-134a	CH_2FCF_3	13.8	3300	1300	400
HFC-143	CHF_2CH_2F	3.4	1100	330	100
HFC-143a	CF_3CH_3	52	5500	4300	1600
HFC-152	$CH_2\,FCH_2F$	0.5	140	43	13
HFC-152a	CH_3CHF_2	1.4	410	120	37
HFC-161	CH_3CH_2F	0.3	40	12	4
HFC-227ea	CF_3CHFCF_3	33	5600	3500	1100
HFC-236eb	$CH_2FCF_2CF_3$	13.2	3300	1300	390
HFC-236ea	CHF_2CHFCF_3	10	3600	1200	390
HFC-236fa	$CF_3CH_2CF_3$	220	7500	9400	7100
HFC-245ca	$CH_2FCF_2CHF_2$	5.9	2100	640	200
HFC-245fa	$CHF_2CH_2CF_3$	7.2	3000	950	300
HFC-365mfe	$CF_3CH_2CF_2CH_3$	9.9	2600	890	280
HFC-43-10mee	$CF_3CHFCHFCF_2CF_3$	15	3700	1500	470
Fully fluorinated species					
SF_6		3200	15100	22200	32400
CF_4		50000	3900	5700	8900
C_2F_6		10000	8000	11900	18000
C_3F_8		2600	5900	8600	12400
C_4F_{10}		2600	5900	8600	12400
c-$C_4\,F_8$		3200	6800	10000	14500
C_5F_{12}		4100	6000	8900	13200
$C_6\,F_{14}$		3200	6100	9000	13200
Ethers and Halogenated Ethers					
CH_3OCH_3		0.015	1	1	<< 1
HFE-125	CF_3OCHF_2	150	12900	14900	9200
HFE-134	CHF_2OCHF_2	26.2	10500	6100	2000
HFE-143a	CH_3OCF_3	4.4	2500	750	230
HCFE-235da2	$CF_3CHClOCHF_2$	2.6	1100	340	110
HFE-245fa2	$CF_3CH_2OCHF_2$	4.4	1900	570	180
HFE-254cb2	$CHF_2CF_2OCH_3$	0.22	99	30	9
HFE-7100	$C_4F_9OCH_3$	5.0	1300	390	120
HFE-7200	$C_4F_9OC_2H_5$	0.77	190	55	17
H-Galden 1040x	$CHF_2OCF_2OC_2F_4OCHF_2$	6.3	5900	1800	560
HG-10	$CHF_2OCF_2OCHF_2$	12.1	7500	2700	850
HG-01	$CHF_2OCF_2CF_2OCHF_2$	6.2	4700	1500	450

When the size of scattering source becomes several orders of magnitude larger than the wavelength the scattering can often be replaced by simple reflections (approximation for geometric optics), but still surface properties and edges can cause additional scattering into other directions. There have been several methods developed for such computations, since the scattering of radiation is of high importance in various scientific and technological applications. The absorption by the gases mentioned above, by clouds and by aerosols can be simulated in radiative transfer codes (see next section), where the respective absorption properties of these species are now available in data libraries, given also below. There is a very large variability of the absorption and scattering properties of aerosols and cloud particles due to their chemical composition, size and also shape (e.g.: 99Tho). In remote sensing applications near the earth's horizon also the refraction within the atmosphere must be considered.

4.2.4 Major radiative transfer codes and data libraries ready for use

There are now well-proven data banks available containing not only various radiative transfer codes but also examples of model atmospheres. Moreover, they contain in various detail information on the spectral absorption characteristics of a large variety of atmospheric gases. These are in particular the data banks MODTRAN (93And), GEISA (92Hus) and HITRAN (98Rot). They are continuously subject of updating and available in the internet (e.g.: http://www.hitran.com). Other radiative transfer codes, in particular those used in climate models, are subject of steady intercomparison by the respective user groups.

For more operational use such details are often averaged over larger spectral ranges with the effect, that such codes may loose accuracy. There are, however, intensive efforts to "calibrate" them.

4.2.5 The atmospheric greenhouse effect

The expression "atmospheric greenhouse effect" is a misnomer, since a real greenhouse or winter garden shields the inside also from turbulent exchanges of air with the outside, while our atmosphere is "open to space" and can only exchange radiant energy. However, the major greenhouse gases (water vapor, carbon dioxide, methane, nitrous oxide, ozone and the various CFCs) act quite similar. They are almost completely transparent (exceptions are: water vapor in the solar infrared and ozone in the UV and quite less ozone in the visible portion of the spectrum) for the short-wave solar radiation. However they absorb and re-emit very efficiently with their own temperature the long-wave heat radiation.

As a net-effect the ground and the lowest layers of the atmosphere are heated while the upper ones are cooled. This is the main reason for the mean decrease of temperatures in the troposphere with increasing height. The strong absorption of the high energetic ultraviolet (UV) radiation by stratospheric ozone causes the increase of temperatures in stratospheric layers above the tropopause (at about 7 to 17 km) up to the stratopause (near 50 km), where again radiative cooling to space by the Greenhouse gases begins to dominate. Stratospheric ozone absorbs in its 9.6 μm band also a small fraction of heat radiation emitted from the surface to space. Clouds, aerosols and the surface properties alter regionally very strong this general picture according to their own radiative transfer properties. Their occurrence is also dependent on the time of the day. They absorb only a small amount of incoming solar radiation but they reflect back to space more than the clear atmosphere (see section 4.3). On the other side, clouds (aerosols much less) absorb almost all long-wave terrestrial radiation originating from below and emit with their own base-temperature radiation back to the surface, thus preventing our planet's surface from cooling to space.

A rather simple solution of the radiative transfer equation has been used by Manabe and Strickler (64Man) to demonstrate that the vertical temperature profiles in a static atmosphere can easily be simulated. They are shown in Fig. 4.2.5.1, for pure radiative equilibrium, for a dry adiabatic adjustment and for a mean constant vertical temperature gradient of 6.5 K/km in the troposphere. These curves reproduce the observed profiles quite well.

The so-called "**anthropogenetic Greenhouse effect**" is caused by the well documented increase of CO_2, CH_4, ozone and N_2O, whose concentrations in the troposphere rose from the pre-industrial time (around 1850) to the present by about 30%, 160% and 40% of their previous values, while the stratospheric ozone concentration decreased since about 1970. Also the many CFCs and their replacements, as summarized in Table 4.2.2.1, are assumed to enhance the Greenhouse effect. A very small increase of the lower tropospheric water vapor has also been found (see IPCC 2001 and also Chapter on Water Vapor in this volume) while the lower stratospheric water vapor mixing ratio may have

increased by about 50% since the year 1960 (03Ros). It can be shown that these changes increase the radiative heating of lowest tropospheric layers and the cooling in the upper troposphere and in the stratosphere.

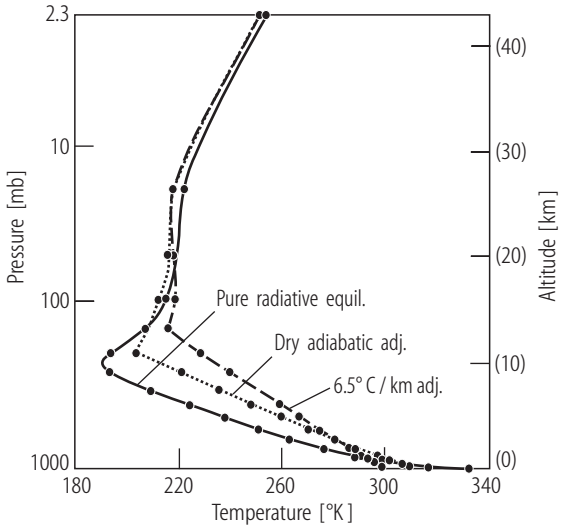

Fig. 4.2.5.1 Temperature profiles which would occur in the atmosphere for pure radiative equilibrium between Earth and space, and for dry adiabatic and constant vertical gradient of 6.5 K/km adjustment in the troposphere (from (64Man)).

4.3 An overview on the radiation budget of the climate system

4.3.1 Annual budget

An overview on our present knowledge of the radiation budget in the climate system is shown in Fig. 4.3.1.1 (from 98Ohm, based on earlier work by 97Ohm and 98Wil). The values given in this diagram are based on information extracted from at that time known satellite products and from ground-based measurements. Numerous similar diagrams have been published by different authors (e.g. (97Kie)), where often the fractional amounts of redistributed components in the atmosphere differ only slightly. Their computation is based on a mean annual value of the solar constant (Sect. 3.2) of 1368 Wm^{-2}, where due to spherical shape of the Earths only ¼ reaches the top of the atmosphere (see also section 4.3.2 of the chapter).

A schematic overview of the net heating and cooling by the solar and terrestrial radiation fluxes (RAD) in the troposphere and in the lower stratosphere for mean climate conditions (as known at that time, around 1982) has been provided by Webster and Stephens (84Web). It is shown in Fig. 4.3.1.2 and illustrates, where low and high clouds play a particular role in the radiative and condensational heating and cooling of the atmosphere.

The release of heat of condensation by the formation of clouds heats the troposphere. The total net cooling of the troposphere by radiation, even at lower layers (for the present temperature fields) must be compensated by eddy and turbulent heat transports (Q_{EDDY}) at the surface.

4.3.2 Solar radiation

The "solar constant" symbolizes the total radiative flux density of electromagnetic radiation emitted from the Sun into space and arriving at the top of the atmosphere at mean distance sun/earth (1 AU: Astronomical Unit). It is now adopted in many model studies and textbooks to be about 1368 Wm^{-2} ± 1 Wm^{-2}. During the past 30 years many airborne and satellite measurements confirmed the existence of a slight variation due to the 11-year solar cycle of the order of about ± 0.6 Wm^{-2} as shown in the time series by Lean (00Lea), Froehlich and Lean (98Fro) and Quinn and Froehlich (99Qui) in Fig. 4.3.2.1, where also more recent data have been added. Their preferred value for the present irradiance of the Sun is about 1366.5 ± 0.6 Wm^{-2}.

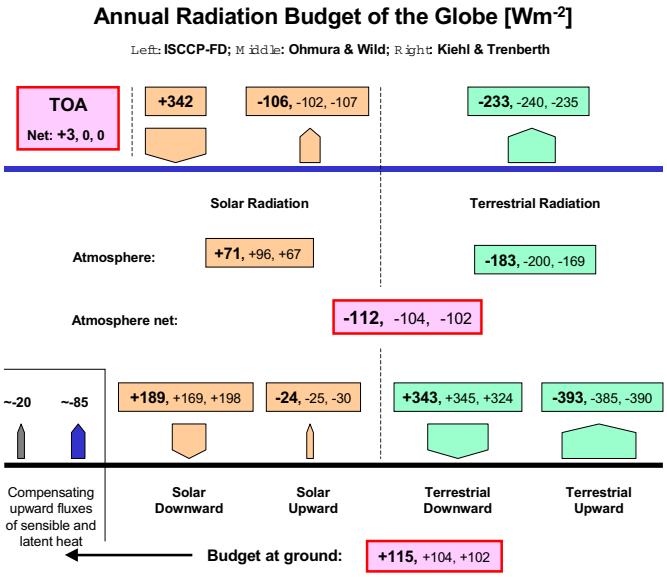

Fig. 4.3.1.1 Redistribution of radiative energy in the climate system (from 05Ras). All values refer to a mean solar constant of 1366 Wm^{-2} and are global annual averages. Note the large amount of surplus heat at the surface, which must be removed from the surface by turbulent fluxes of latent and sensible heat. The radiation budget of the atmosphere alone is negative, requiring an amount of about 104 Wm^{-2} to be added from ground by evapotranspiration and fluxes of sensible heat. These values are the new values from the ISCCP data set and from other sources in Table 4.3.6.1.

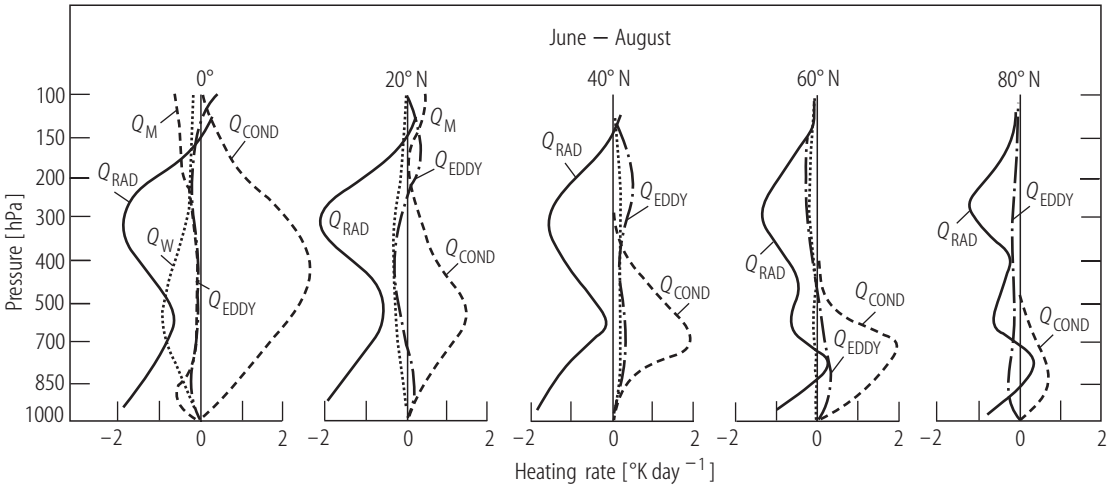

Fig. 4.3.1.2 Zonal averages of heating rates in K/day by radiation (RAD), by eddy fluxes (EDDY) and by latent heat (COND), estimated from climate data (from 84Web). Note, that Q(RAD) is negative, since the atmosphere is loosing more radiant energy to space than it absorbs. The cooling peaks were most cloud surfaces are located and Q(COND) peaks were most clouds are formed. The vertical coordinate is given in hPa. Q(M) and Q(W) are the mean adiabatic heat convergences, respectively.

This short time series of direct space-borne measurements could be used together with long recordings of the sunspot number and various data such as on the abundance of the isotopes ^{14}C and ^{10}Be, to establish a time series of the solar constant variability during the past about 1.000 years. This extended series is now used in various numerical studies of the past climate states and is shown in Fig. 4.3.2.2 (from 00Cro).

These curves show an almost equal amplitude of the solar irradiance during the recent times and the middle age between the years 1000 and 1200, while during the 16th and 17th century, the Spoerer, Maunder and Dalton Minimum of Sunspot activities, the Sun emitted somewhat less radiation affecting also the Earth. The present very small increase of the Solar Irradiance does not completely explain the global warming occurring during about the last 50 years.

Changes in the sunspot density cause also slight changes in the spectral composition, which are most prominent in the UV and at shorter wavelengths, where solar radiation is completely absorbed in the upper atmosphere. This may even influence the ozone layer in the stratosphere and feed then back to the main wind patterns in the upper troposphere, which in turn can control the position of upper tropospheric jet streams in the middle latitudinal areas of the Earth.

The spectral variations are in particular very high in the UV portion of the spectrum and at smaller wavelengths (00Lea)). They are shown in Fig. 4.3.2.3.

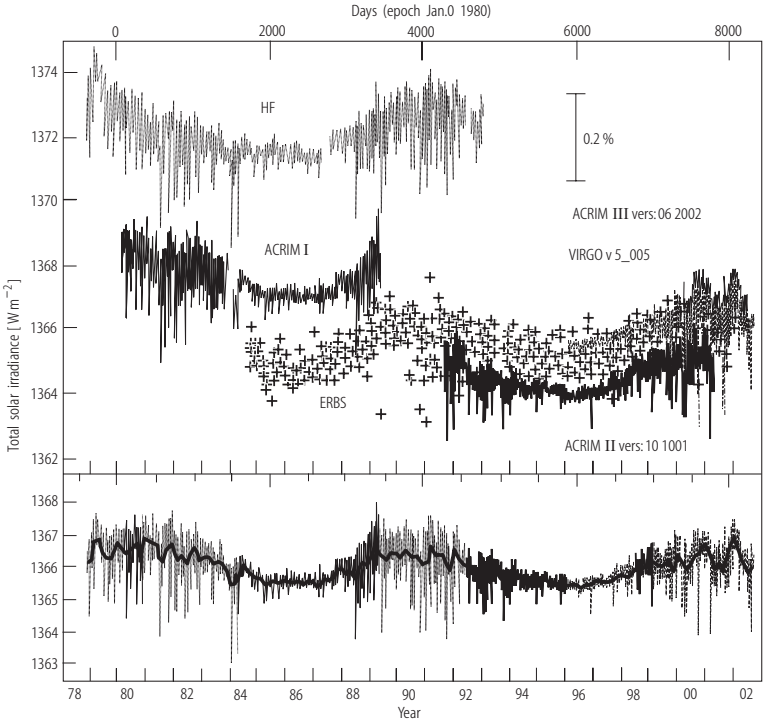

Fig. 4.3.2.1 Bottom: Measured time series of the Sun's irradiance at 1 AU, as obtained with different instruments from different satellites and adjusted to the Space Absolute Radiometric Reference. Note the strong variability during periods of maximal solar irradiance. In the top panel are shown the original measurements. They were made from different satellites. The systematic shifts in scales are due to problems in absolute calibrations. A new value for the present solar irradiance of 1366.5 Wm^{-2} is assumed. These figures are updated versions from Froehlich and Lean (98Fro), and from Quinn and Froehlich (99Qui), respectively.

Since our Earth orbits around the Sun like a gyre with a slightly tilted axis and moves on an elliptic orbit, there are several astro-mechanical causes for the seasonal and longer period changes in the insolation, which are affecting also our climate. These were described by M. Milankovic and made responsible for the periodic occurrence of major glacial periods of about 100,000 years on Earth as they were found in Antarctic Ice cores (e.g. (99Pet)). These astro-mechanical influences on the solar radiant energy at the top of the atmosphere are described in many textbooks on atmospheric sciences or climatology.

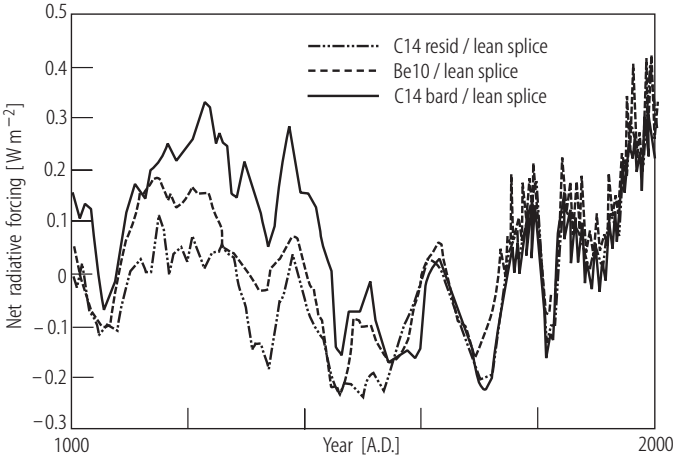

Fig. 4.3.2.2 Variation of the Solar Constant or extraterrestrial solar irradiance during the past 1000 years, as derived from different proxy data. Note the high values in the 11th and 12th century, which might have caused the "Medieval Warming" (from Crowley (00Cro)). Units are deviations from an average.

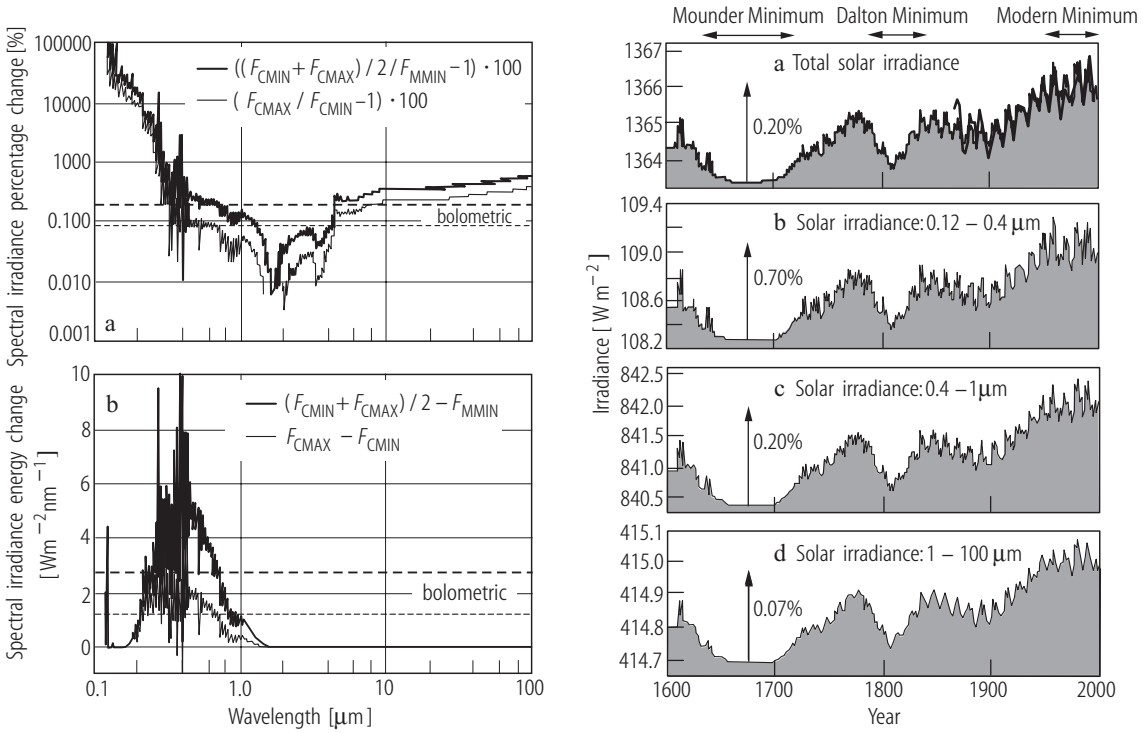

Fig. 4.3.2.3 Left panel: Estimated spectral variations of the Sun's irradiance due to variations in the sunspot activity between the solar cycle minimum (CMIN) to the maximum (thin line) and from the Maunder Minimum (MMIN) to the present solar cycle (thick line). Right panel: Reconstructions of annual total and of broad-band irradiances (11 year running means are the grey areas) for the period 1600 to 2000. Arrows show the percentage increases from the year 1675 to the mean of cycle 22 (1986 to 1996), from (00Lea).

Several possible extraterrestrial forcings of our climate have recently been summarized by Reid (00Rei). These are the effects of changes of the UV component (see above) on the heat budget in the middle and lower stratosphere, the possible effects of changing blue component in the visible light on heating deeper (20 to 40 meters) ocean layers and also the modulation of Galactic Cosmic Rays (GCR) by the Sun's magnetic fields. The latter may affect the cloud formation by charged condensation and ice nuclei (see also 02Car and 03Har). However several statistical findings of relations between the occurrence of clouds and the intensity of GCR need further and more convincing explanation.

4.3.3 Radiation budget at the top of the atmosphere (TOA)

4.3.3.1 Definitions and basic data

As already mentioned above we prefer in this monograph to describe the present knowledge on the radiation budget and on clouds with the data set of the International Satellite Cloud Climatology Project (ISCCP: see e.g. (99Ros)). This information is based on a thorough analysis and recalibration of the operational narrow-band imagery data from various geostationary and polar orbiting satellites, which is used to identify clouds and other quantities. We provide a brief error analysis at the end of this section 4.3.3. The analysis procedure is based on the well calibrated spectral radiance data of the ISCCP (see chapter on clouds), which is collected from all operational meteorological satellites. These spectral radiances, mostly measured in the visible portion and in the thermal infrared portion of the spectrum, must be converted into up- and down welling radiation flux densities, now representing the entire spectral ranges of the solar (between wavelengths of 0.3 and 4 μm) and terrestrial (between wavelengths of 4 and about 50 μm) radiation.

The up- and downward broad-band fluxes of solar short-wave and terrestrial long-wave radiation **are calculated** with the cloud information extracted from the ISCCP radiance data. For this purpose further specific input data are needed on daily atmospheric profiles of humidity and temperature, on the daily ozone abundance, on the cloud vertical layer distributions, of cloud particle sizes and stratospheric aerosol and ozone. Further climatological data is added on the diurnal variation of near-surface air temperature, on the vertical cloud distribution, on the tropospheric aerosol and also on the spectral surface albedo and emittance. Values of the cloud effects are determined as differences between those for clear and cloudy sky, where positive values mean an increase of radiative fluxes, etc. **In summary, this data set on the radiation budget of the planet and its atmosphere is entirely based on calculations with actual and climatological input data.**

The results presented here in all maps are available with a horizontal resolution of 280 km only. The inclusion of geostationary observations into the ISCCP data set enabled a quite complete correction for diurnal variations of radiation fluxes and clouds.

Basically we define the radiant energy **incoming from space** as **positive (**see more details also **in the legend to Fig. 4.1.1)**, considering the Earth as a planet being heated only by the Sun. Internal sources are 5 to 6 orders of magnitude smaller than the Sun's irradiance (see summary in 72Ras). All fluxes into the opposite direction are signed as negative. We show in this chapter only maps of annual averages. Seasonal variations are shown in the Appendix to this Chapter.

4.3.3.2 Mean global fields

This information on the various components of the radiation budget at the top of the atmosphere, TOA, where this level can be assumed at an altitude of about 50 to 100 km, is presented below. The net radiation at this level is also called the planetary radiation budget. This quantity is not only important for basic climate studies, but also for the validation of the energy budget and of various influences on it as simulated in the models for our climate system (e.g. 95Wie). In Figs. 4.3.3.1 to 4.3.3.4 are shown as a first result maps of the radiation budget components at the top of the atmosphere (TOA). Note in Fig. 4.3.3.4 the small annual deficit over the bright and hot desert regions in North Africa and East Asia. Elsewhere between about 35 degrees latitude on both sides of the equator the earth earns more radiative energy as it emits back to space. Global averages are summarized in Table 4.3.2. Strong deficits in the budget occur over both Polar Regions.

The basic importance of this heat budget for the understanding of our climate is underlined by the fact that already at the end of the 19-th century first estimates were made on basis of the at that time very scarce information on the climate of the earth, in particular on clouds. Later, as more data became available inclusive observations of the Earth's reflection to the Moon, many estimates followed until the first satellite data became available in the earlier 1960-th.

There have been during the past 40 years many special radiometers designed to measure the radiation budget of the earth aboard a satellite. Basically they measure the upward directed flux density of the solar and the total (i.e. solar plus terrestrial) radiation from the whole disc of the Earth as seen from a satellite or the upward radiances of solar, terrestrial and total radiation. The latter instruments allow for higher spatial resolutions of 50 km and better on Earth which is important for regional climate studies. The analysis of such data, however, requires a thorough knowledge of the angular dependence of the spectral composition and total intensity of upward radiances emerging from different "targets" on earth. Such information could be derived now from many measurements made in the past.

The results shown here were calculated from the ISCCP data set, which is storing mostly spectrally higher resolved measurements of operational imagers and various ancillary data. They agree, however, globally and also regionally quite well (globally within 2 to 5 Wm^{-2}, regionally poorer) with those derived from other and more dedicated measurements. Special radiometers to measure specifically the components of the radiation budget at TOA are now flown onboard of several operational and experimental satellites, since this information is of basic importance for the calibration of global circulation models (95Wie). In Fig. 4.3.3.5 is made a comparison of the required poleward transport of energy within the climate system with estimates of the same quantity obtained from data of the earlier Earth Radiation Budget Experiment (ERBE). This meridional transport is performed by the atmosphere and oceans. The agreement between both data sets is quite satisfactory.

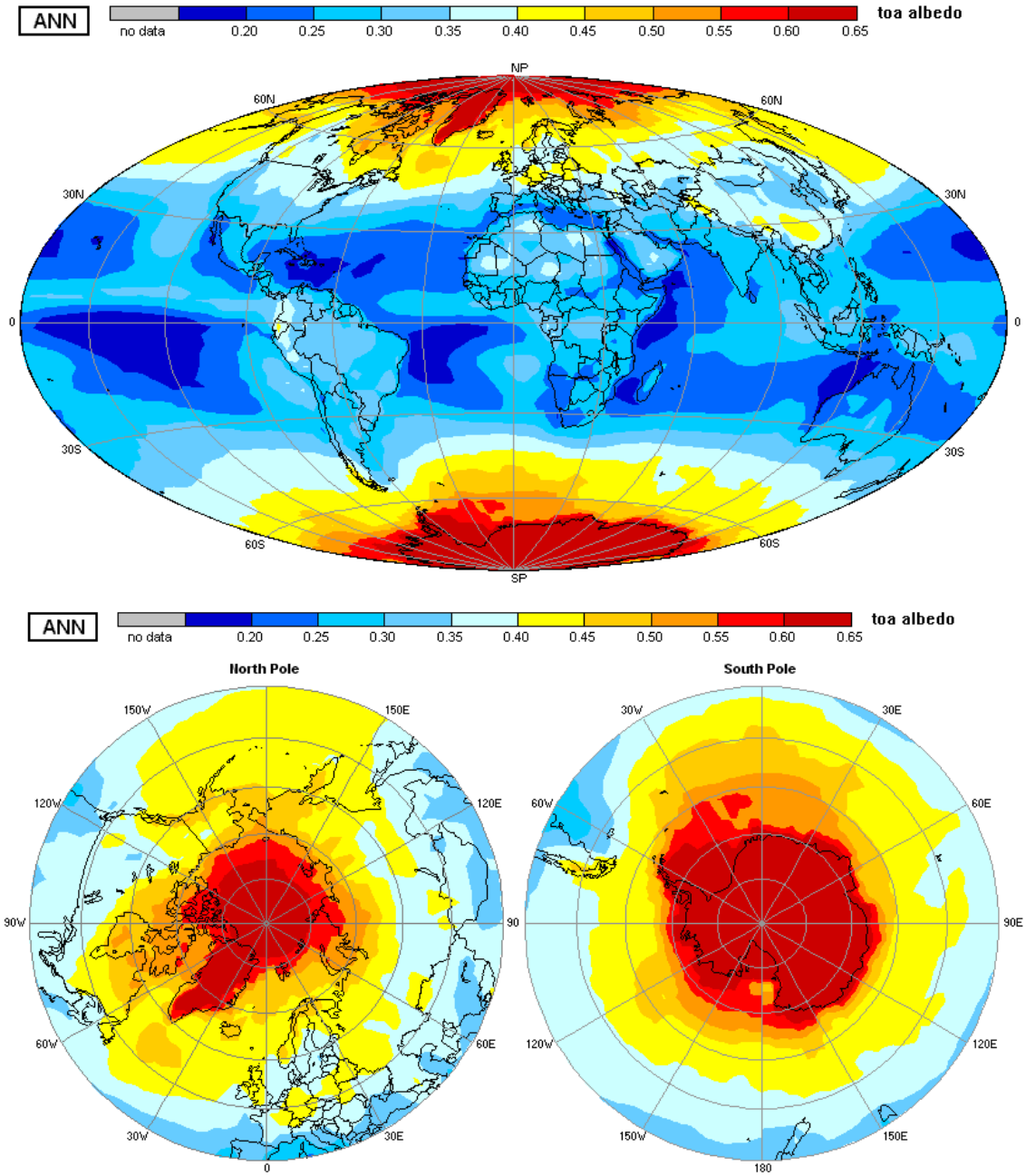

Fig. 4.3.3.1 Annual averages of the albedo of the earth-atmosphere system (= reflected divided by incident solar radiation, where the latter can easily be computed from the solar constant and other information on period and location) **during the period 1991 to 1995**. This distribution is due to different albedo of oceans and continents and of the cloud field distribution. Highest value: 0.68; lowest value: 0.16; global average: 0.31. The reflectance of clouds, continents and ice and snow fields modulates dominantly these fields.

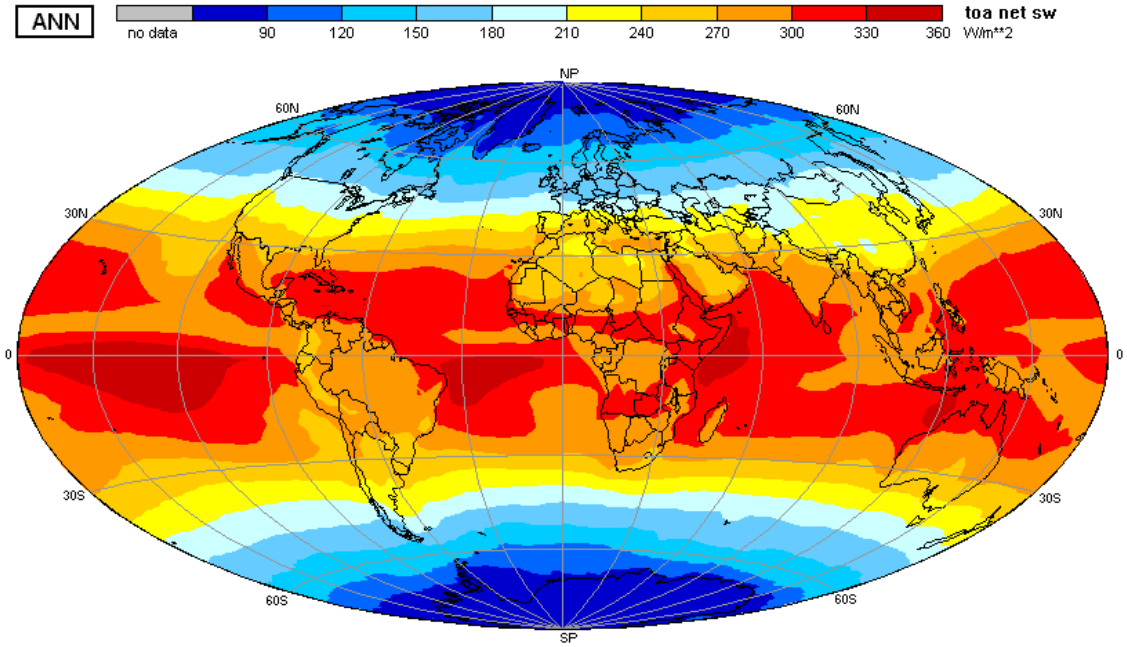

4.3.3.2a Annual averages of the solar net radiation at top of the atmosphere (or (1.0 − albedo) × incident radiation) **in Wm^{-2}** of the period 1991 to 1995. This quantity is equivalent to the amount of solar radiation absorbed in the earth-atmosphere system. Due to the low surface albedo and the relatively small cloudiness, the subtropical ocean areas gain highest amounts of solar energy. Highest and lowest values are 352 and 56 Wm^{-2} ; global average: 236 Wm^{-2}.

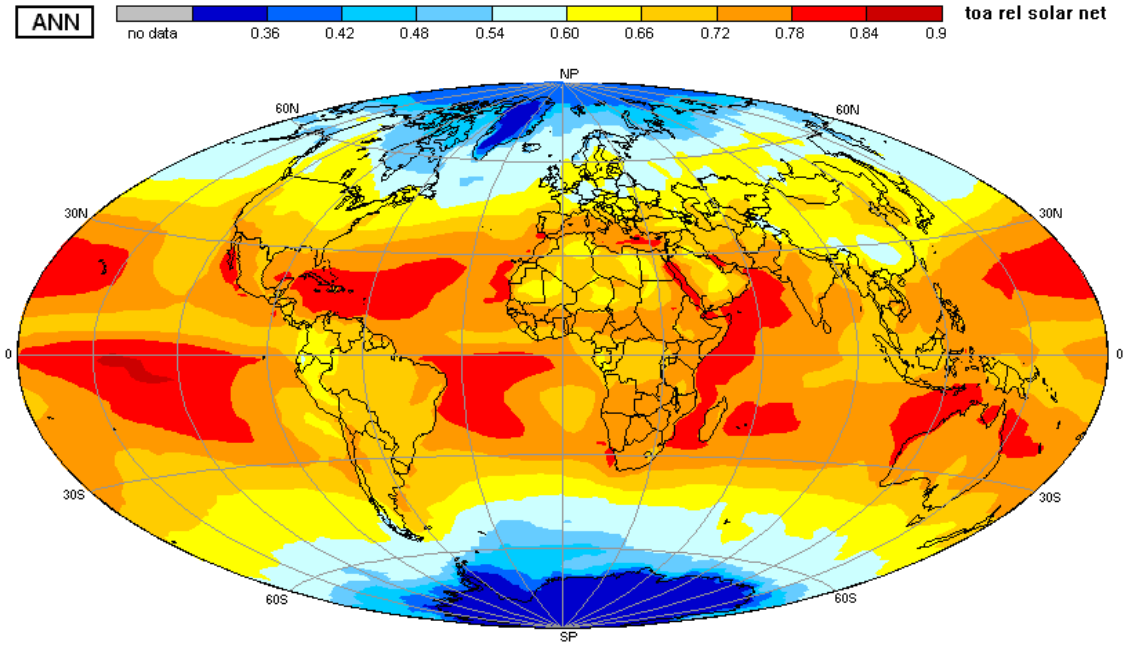

Fig. 4.3.3.2b Annual averages of the relative absorption of solar radiation in the climate system, related to the incoming solar radiation. This quantity has been computed to enhance the regional variability due to surface albedo and cloud fields and to reduce the zonality due to the earth's shape. The dark red areas indicate that more than 78 % of the incoming radiation is absorbed in the climate system. Highest and lowest values are 0.84 and 0.32; global average: 0.69. All values are for the period 1991 to 1995.

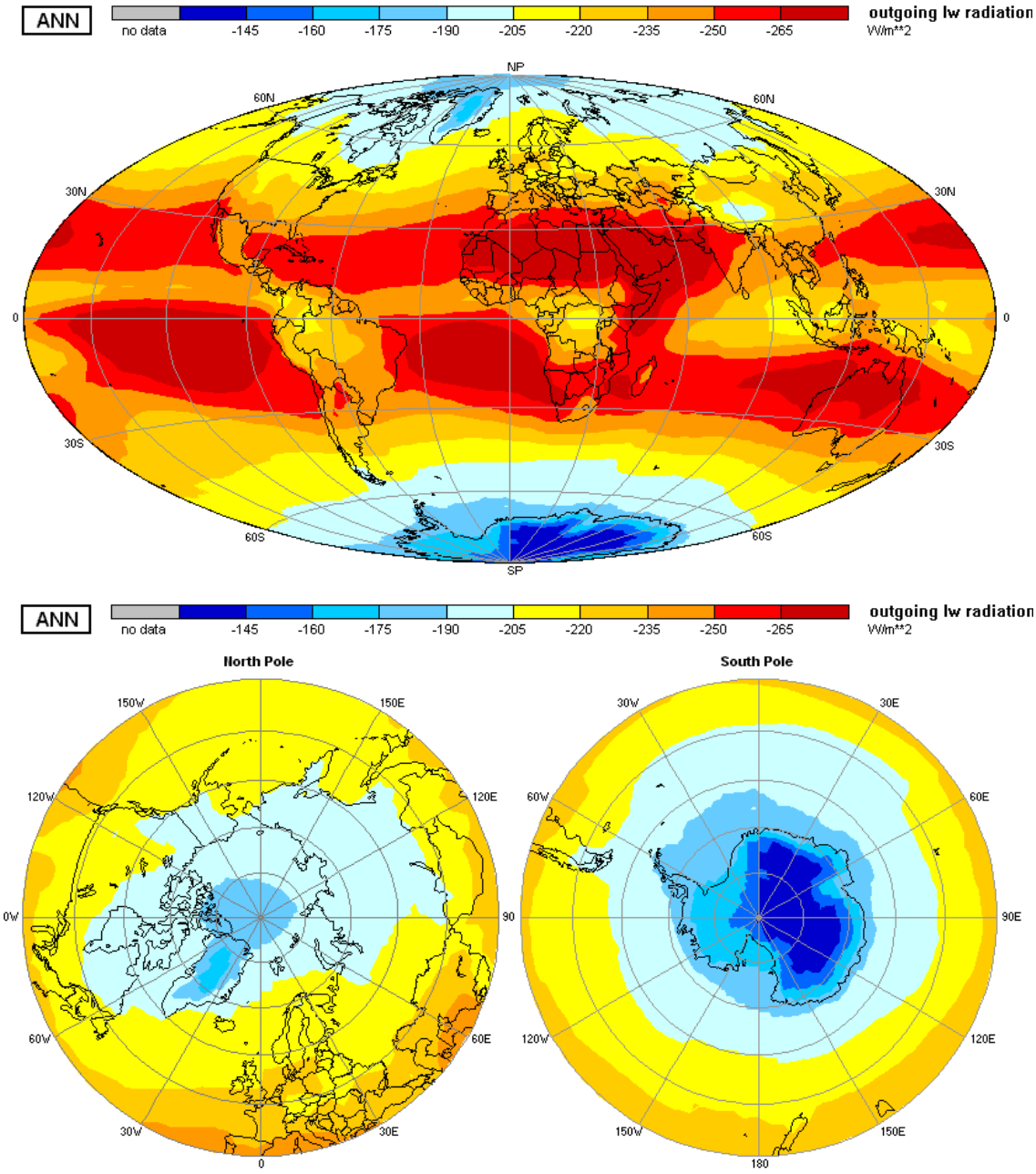

Fig. 4.3.3.3 Annual averages of the outgoing terrestrial radiation at top of the atmosphere in Wm^{-2} for the period 1991 to 1995. Note the effect of the high tropical cloud systems shielding entirely the warmer surface and emitting much less radiation with their own surfaces, which are much colder than the earth's surface underneath. Lowest emissions occur over the Antarctic Plateau. Areas of highest emission are observed over both subtropical belts. Note also the "hot spots" over the Arabian and African deserts and over the subtropical southern Pacific Ocean. Highest emission to space: –286 Wm^{-2}; lowest emission: –124 Wm^{-2}; global average: –233 Wm^{-2}.

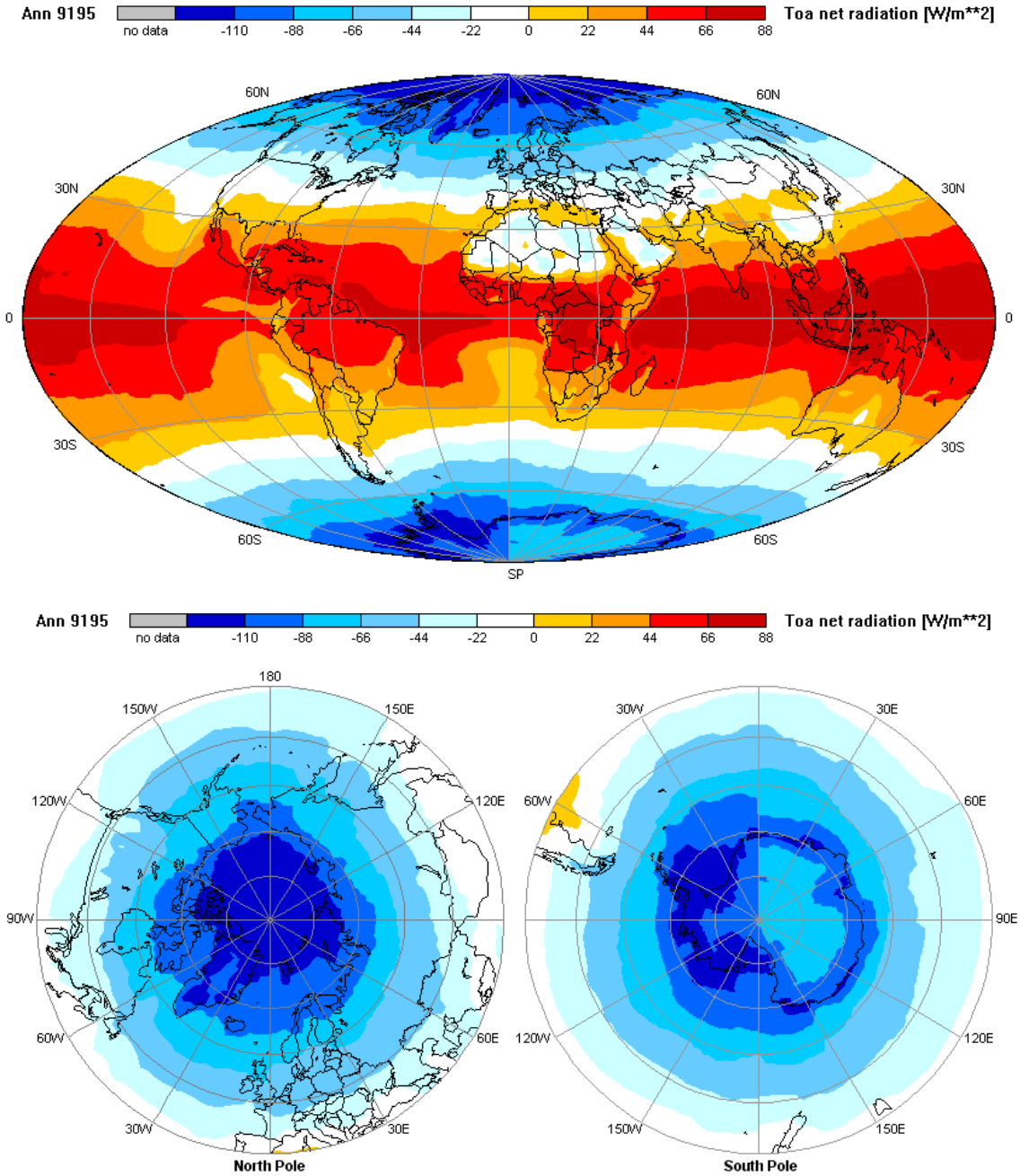

Fig. 4.3.3.4 Annual averages of the net radiation at top of the atmosphere or "planetary radiation budget", in Wm^{-2} for the period 1991 to 1995. Its components are the incoming and reflected solar radiation and the outgoing terrestrial radiation. Over all yellowish and red areas the net solar radiation is higher than the outgoing terrestrial radiation. Over all bluish areas the terrestrial emission of heat radiation to space dominates. These individual components are shown in the following figures. Highest deficit: –126 Wm^{-2}; highest gain: +88 Wm^{-2}; global average: +3 Wm^{-2}. This global surplus **cannot** be interpreted as a forcing of the present global warming, since it is within the uncertainty range of such calculations.

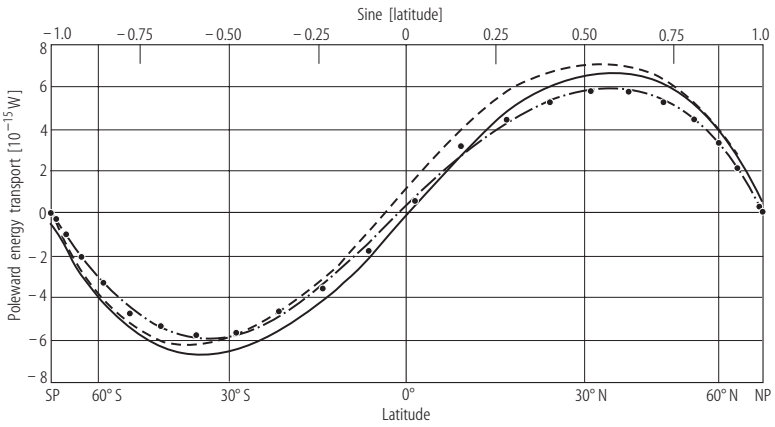

Fig. 4.3.3.5 Mean annual required poleward energy flux (in 10^{15} W), calculated from the zonal averages of the planetary radiation budget (see map in Fig. 4.3.3.4) and compared with values (dashed dotted curve and dots) of the earlier Earth Radiation Budget Experiment ERBE (Fig. 7.16 in (94Har)). The dashed (integration from S to N) and full (integration from N to S) curves deviate slightly, since the global budget from ISCCP data has been calculated to be +3 Wm^{-2}. This value is located within range of uncertainty and cannot be interpreted as a forcing of the present global warming. In comparison between both results, the ISCCP data seem to overestimate the poleward heat transport.

4.3.3.3 Effects of clouds on the planetary radiation budget

These budget components, except the incident solar radiation, are highly influenced by clouds. Other contributions originate from albedo and temperature of the Earth's surface and from the atmospheric composition and temperature. The **cloud effect** (also called: cloud radiative forcing) can quantitatively be estimated from such measurements determining for a particular period firstly the fields for "clear skies" and subtracting them from the averages shown above. The observational period must be short enough to avoid significant seasonal trends. With this convention (cloudy minus clear) we obtain **negative values, when clouds decrease** and **positive values, when clouds increase** a flux component. In our data also the radiation fields are calculated for a cloud free atmosphere. Since the "clear sky – standard" can only consider a mean aerosol content, this cloud effect contains also effects of additional aerosols over areas of anomalous high aerosol in the atmosphere. Since in these calculations none of the usual anomalies in aerosol distributions, which are due to desert storms, biomass burning and other (often human) effects can be considered in detail, the "cloud effect" may also be influenced by them. Some earlier results, which were derived from earlier measurements of the planetary radiation budget components by the Earth Radiation Budget Experiment (ERBE: (90Har)), are shown in Fig. 4.3.3.6 (from (93Hob)). They demonstrate that clouds in all climate zones "keep" terrestrial heat radiation in the climate system (positive values); but they generally reflect a higher amount of incident solar radiation to space. As a net effect clouds tend to "cool" the climate system. The respective global averages obtained from the ERBE data sets, are summarized in Table 4.3.2.

Table 4.3.3.1: Global averages of the radiation budget components at TOA and the effects of clouds (last column) on the outgoing terrestrial radiation, computed from earlier ERBE data (**from 93Hob**). The most recent information of this ISCCP data set is summarized in **Table 4.3.6.1**. The small positive value of the net radiation is considered within the error range of this analysis **and should not interpreted as a heating of our planet.**

Quantities at top of the atmosphere (TOA)	Mean values	For cloudless earth	Effect of clouds
Outgoing terrestrial radiation	–234 Wm^{-2}	–266 Wm^{-2}	+32 Wm^{-2}
Absorbed solar radiation	239 Wm^{-2}	288 Wm^{-2}	–49 Wm^{-2}
Net radiation	+5 Wm^{-2}	+22 Wm^{-2}	–17 Wm^{-2}
Albedo	30%	15%	+15%

For the zonal, annual and global averages it has been found from these earlier data, that clouds generally increase the planetary albedo from about 15% (cloud free planet) to 30%, which corresponds to a reduction of the absorbed solar energy by about 49 Wm^{-2}, but they reduce the emission to space from 266 Wm^{-2} to 234 Wm^{-2}. Thus in summary they contribute to a small decrease of the planetary radiation budget by about –17 Wm^{-2}. Similar vaues are obtained from the ISCCP data sets (Table 4.3.6.2).

The ISCCP results are shown below. There are indeed strong regional variations due to the albedo of the surface, the temperature fields and the cloud field structure and height. Figs 4.3.3.7 to 4.3.3.9 show the respective geographical distributions of the **effect of cloud fields** on the absorption of solar radiation, on the outgoing terrestrial radiation and on the net radiation. They also were obtained from the ISCCP data set. The related seasonal averages are shown in the appendix to Section 4.3.

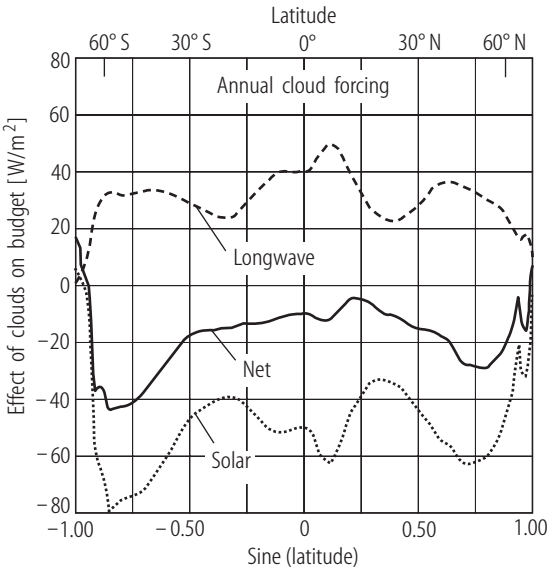

Fig. 4.3.3.6 Earlier estimates of the effect of clouds on the budget derived from measurements of the Earth Radiation Budget Experiment (from 93Hob). Respective values obtained for the ISCCP data are shown in Figs. 4.3.4.12 and 13.

The patterns in the map for absorbed solar radiation (Fig. 4.3.3.7) are mainly caused by the reflectance of underlying surfaces of clouds and continents, whereby the high abundance of clouds in the tropics reduces drastically the absorption. Much smaller effects can be seen in areas of small cloud occurrence. The patterns in the maps for terrestrial radiation (Fig. 4.3.3.8) are dominated by cloud altitudes and respective surface temperatures. Strongest reduction of the emission to space is observed again over the high tropical convective systems, but also the areas of major mid-latitude storm tracks reduce the radiative cooling to space.

The effect of clouds on the net radiation at TOA (Fig. 4.3.3.9) is almost everywhere negative, causing a decrease against clear sky values, except over both Polar Regions. There, the small increase is probably unrealistic, since the detection of clouds over those regions and selection of “clear sky values” is not so easy. The smaller areas of increase over tropical Africa and the Northwestern coast of Australia cannot be explained by special cloud features and are in their magnitude within the uncertainty range of this data treatment.

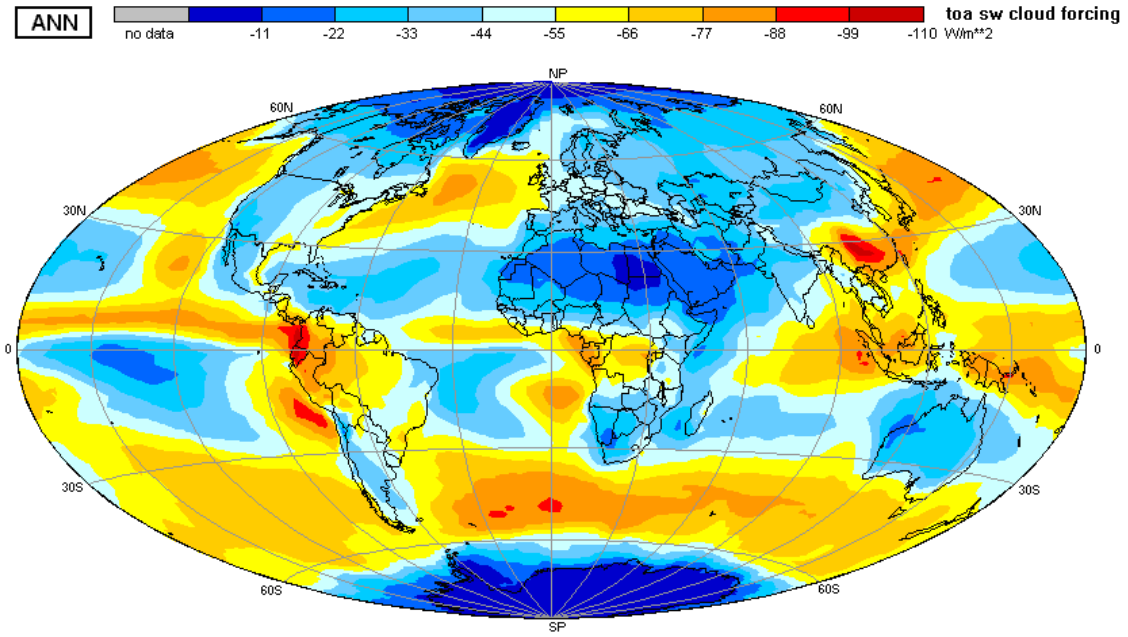

Fig. 4.3.3.7 Annual average of the effect of clouds on the absorption of solar radiation (in Wm^{-2}) within the climate system computed as the difference between the mean values in Fig. 4.3.3.2a and the absorption at clear skies during the period 1991 to 1995. Over the bright deserts and ice and snow fields this effect is very small. All values are negative, since clouds enhance the reflection to space. Highest and lowest values: 0 and 106 Wm^{-2};global average: −50 Wm^{-2}. Although clouds are additional absorbers in the atmosphere, their higher than the ground reflectance is reducing the total absorption. Note the maximum over southern China which also contain the effect of aerosols not considered in these calculations.

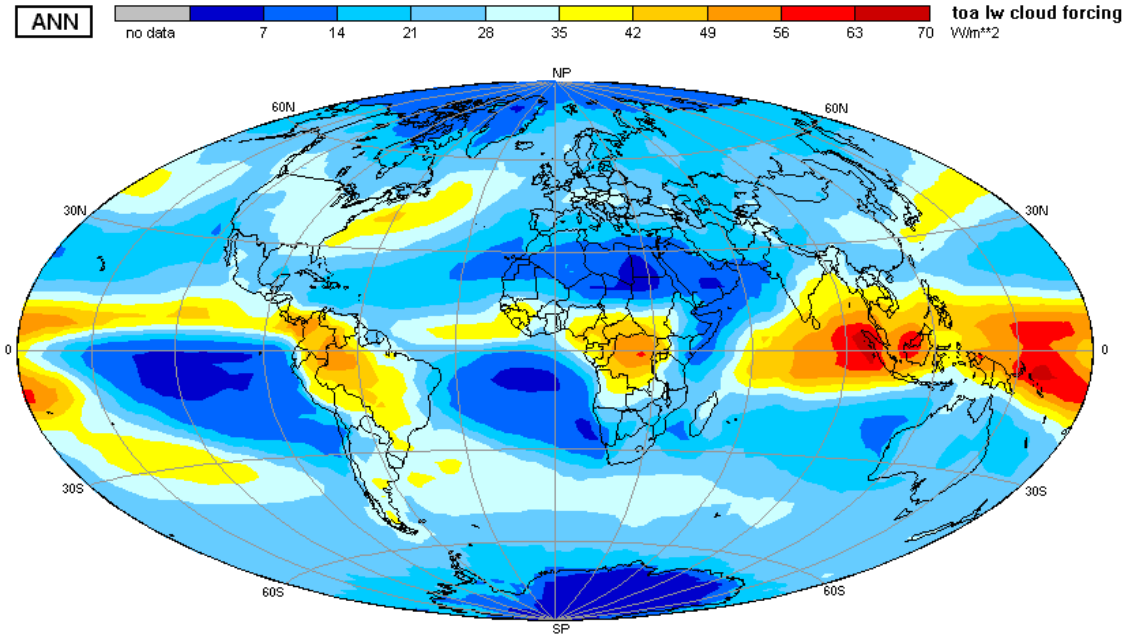

Fig. 4.3.3.8 Annual average of the effects of clouds on the terrestrial radiation (in Wm^{-2}) **leaving the climate system to space** during the period 1991 - 1995, computed as the difference between the mean values in Fig. 4.3.3.3 and the emission at clear skies. **All values are positive**, since clouds generally reduce the emission to space due to their higher and colder surfaces. Highest and lowest values: +70 and +2 Wm^{-2}, global average: +25 Wm^{-2}.

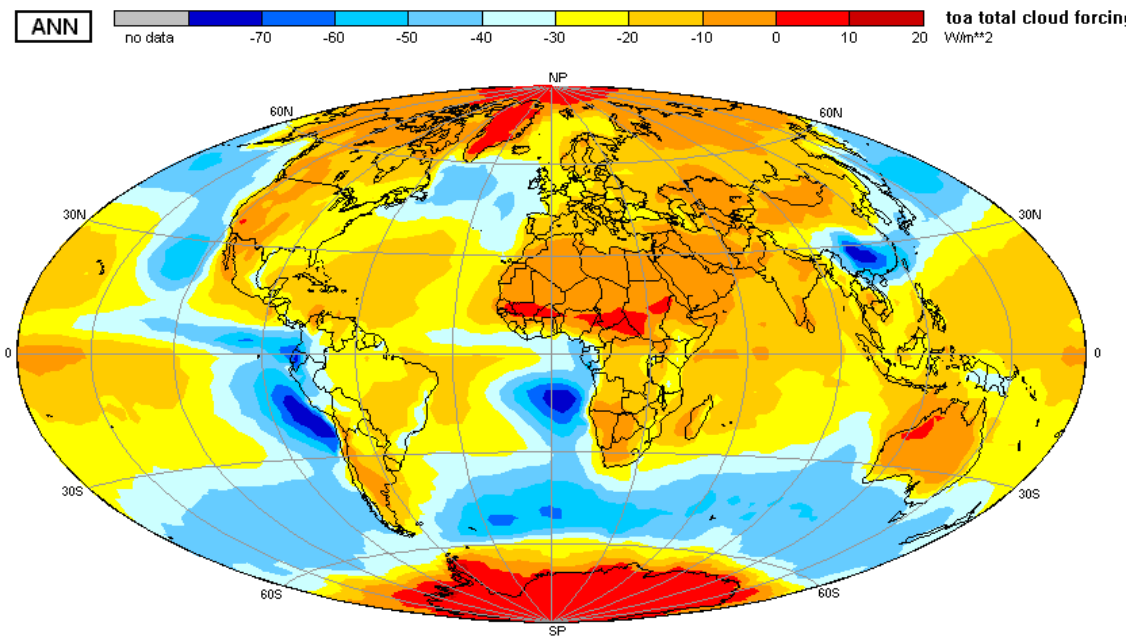

Fig. 4.3.3.9 Annual average of the effect of clouds on the net radiation budget (in Wm^{-2}) during the period 1991 - 1995, computed as the difference between the mean values in Fig. 4.3.3.4 and the net radiation at clear skies. Over most areas clouds tend to reduce the net gain of radiative energy by the climate system (negative values), while over some small areas with high and persistent convection they tend to enhance it. Over both Polar Regions this effect is relatively more inaccurate due to large uncertainties in cloud identifications. Highest and lowest values: +13 and –80 Wm^{-2}; global average: –24 Wm^{-2}.

4.3.4 Radiation Budget at Ground

4.3.4.1 Spectral distribution of downward radiation

Components of the radiation budget at ground are the downward fluxes of total (direct and diffuse) solar radiation and of terrestrial radiation of the atmosphere (with a very small contribution to upward radiation due to reflection), the reflected solar radiation, and the terrestrial radiation emitted from ground. Their net sum, the net radiation at ground, is an essential component of the total energy budget at ground controlling and interacting with other exchange processes (see e.g. Fig. 4.3.1.1). These components can only directly be measured at specific locations over continents, requiring well maintained instrumentation. Over the oceans only a few measurements have been made during specific field campaigns. There are now attempts to measure the downward solar radiation with instruments on buoys.

During the past decades many radiometers for single components or for the net radiation have been developed. For the main purpose to validate relevant data (see below) from satellite information a worldwide network has been established (BSRN: Baseline Surface Radiation Network; see e.g. (98Ohm), and http://bsrn.ethz.ch, http://wrdc-mgo.nrel.gov and http://wrdc.mgo.rssi.ru). The BSRN stations measure also with high accuracy trends in spectral components which might be related to trends in atmospheric properties which are caused by changes in the climate. This network is complemented by several regional networks maintained in a large number of countries. Most of this latter data is collected in the Global Energy Balance Archive (GEBA: 99Gil).

In Fig. 4.3.4.1 and Fig. 4.3.4.2 we show measured and simulated spectra of the downward solar and terrestrial irradiance to demonstrate their complex structure due to different influences of atmospheric gases and of aerosols. Strongest changes in the total spectra of the downward solar radiation at cloud free atmosphere are caused by aerosols in the visible portion of the spectrum in the range between about 0.4 and 0.7 µm, which is also the major part of the photosynthetically active radiation PAR (see Section 4.4). They reduce the direct but enhance the diffuse components of solar radiation reaching the ground.

The downward spectral fluxes of terrestrial or atmospheric radiation (see Fig. 4.3.4.2) show clearly the emission spectra of various atmospheric constituents. Water vapor dominates the downward component at ground, as also shown in the sketch in Fig. 4.1.1. The atmospheric window between about 8 to 12 μm is not completely "clean" due to contributions by a "water vapor continuum" and by various other gases. The upward component at ground depends also on the effective emittance, which is a material property and may vary between values of about 0.8 and 0.995. Most natural surfaces have a mean emittance of about 0.97.

In fact, it is impossible over most continental surfaces to define a correct surface temperature, which may often vary over several degrees over even smaller distances of several 100 meters, depending on the surface structure and its geological properties and on its vegetation and use by man. Therefore, in heat budget studies and in remote sensing of surface temperatures often the expression effective surface temperature is used, relating the measured radiances directly their equivalent black-body temperatures. The satellite integrates correctly over such inhomogeneities within its field of view.

4.3.4.2 Global fields of the components at the Earth's surface

In this section we summarize the maps of the annual averages for the period January 1991 to December 1995 of the downward solar radiation (Fig. 4.3.4.3a and b), of the net flux of solar radiation (Fig. 4.3.4.4), of the downward atmospheric radiation (Fig. 4.3.4.5), of the net terrestrial radiation (Fig. 4.3.4.6) and finally of the total net radiation budget (Fig. 4.3.4.7). In all further considerations all downward flux values are taken as positive and all upward into the atmosphere as negative numbers, respectively, as it has been shown in Fig. 4.1.1.

Maps of the estimated effects of clouds on the net quantities of solar, terrestrial and the net radiation are shown in Figs 4.3.4.8 to 4.3.4.10. Various specific comments to all maps are given directly in their legends.

All these quantities are also result of the computational procedure mentioned above.

To determine the downward solar radiation from other satellite measurements one needs to estimate the effective atmospheric transmittance, which can be done with some a-priori knowledge on the surface albedo and with satellite-borne information on the effective cloudiness over the area of interest. For estimates of the downward atmospheric heat radiation one needs additional information on the lower tropospheric temperature and moisture.

A variety of methods has been developed (see e.g. 98Gil), whose success and accuracy however depends extremely on the availability of simultaneous measurements at ground, since the satellite data provide primarily information on cloud fields as "seen" from space. Direct measurements of cloud boundaries are now provided by the lidar onboard the satellite ICESat.

The surface albedo is determined primarily from satellite measurements at clear skies, when the upward radiance is relatively weak enhanced by the atmosphere and by aerosols. Determinations of the surface temperature also require clear sky observations in the infrared, but over continents estimates are also possible from microwave data. There have been multi-spectral methods developed to reduce the atmospheric effects allowing determinations of the sea surface temperature within an uncertainty range of ± 0.5 K or even better. The mean solar surface albedo map is given in Fig. 4.3.4.13.

In the analysis procedure the radiation fluxes shown in the following figures were carefully compared to a large number of direct measurements, which however are mostly available over continents and some islands. Therefore a conservative estimate of the error budget places all downward solar fluxes, after averaging over the available grid resolution of 2.5×2.5 degrees in the range between 10 to 15 Wm^{-2} and of the downward terrestrial radiation in the range between 15 to 20 Wm^{-2}, where even ground-based measurements themselves are uncertain within ±5 to 10 Wm^{-2}. Averages over the globe are expected to be more accurate.

Operational calculations of these radiation fluxes are now made by several weather services for their clients and also for climate studies. Furthermore several research groups developed algorithms for the calculations of these products from satellite data within the frame of the World Climate Research Program but also for the purposes of the use of solar energy resources. In this presentation, however, we use again the products derived from the ISCCP data set.

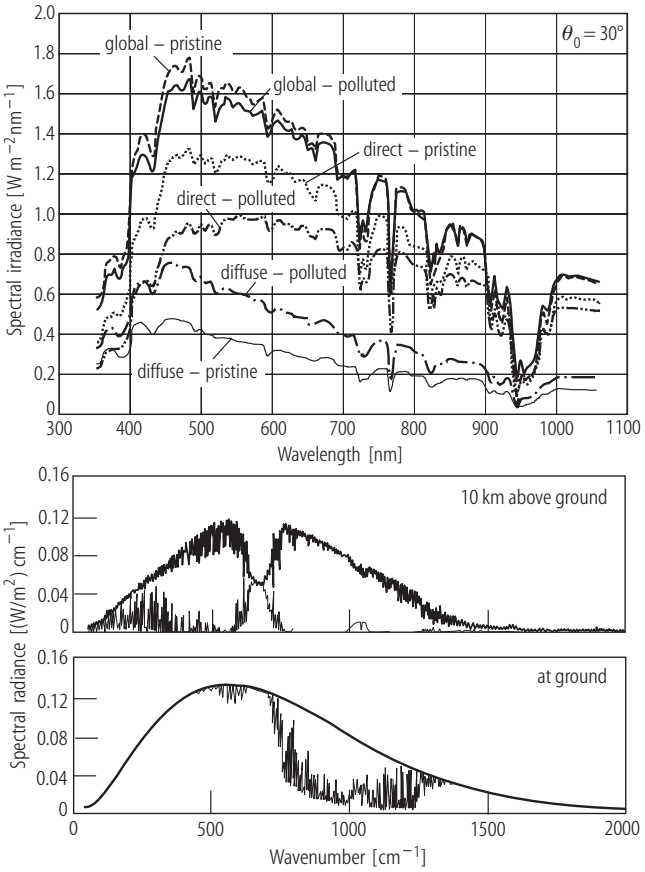

Fig. 4.3.4.1 Measured spectra of downward direct and diffuse solar radiation over the Pacific Ocean (from 98Mey). The measured spectra are obtained at clear skies, but different degrees of pollution by aerosols, at solar zenith angle of 30°. Note, that the additional aerosols increase the diffuse component and reduce the direct component in the visible portion of the spectrum. Spectra like these are now routinely measured at several stations of the Atmospheric Radiation Measurement Program (http://www.ARM.gov) in different climate zones.

Fig. 4.3.4.2 Calculated spectra of the downward (thin line) and upward (thick line) atmospheric heat radiation at ground and 10 km altitude (from R. Hollmann, 2001, private comm.). These spectra show clearly the effects of atmospheric gases, which are schematically indicated in Fig. 4.1.1. At wave numbers smaller than 500 cm^{-1} the atmospheric water vapor dominates the transfer of radiative energy. Wavelength in μm can be computed from 10^4 times of the reciprocal wavenumber (1/wavenumber). Ordinate: spectral radiances in W/m^{2}cm^{-1}.

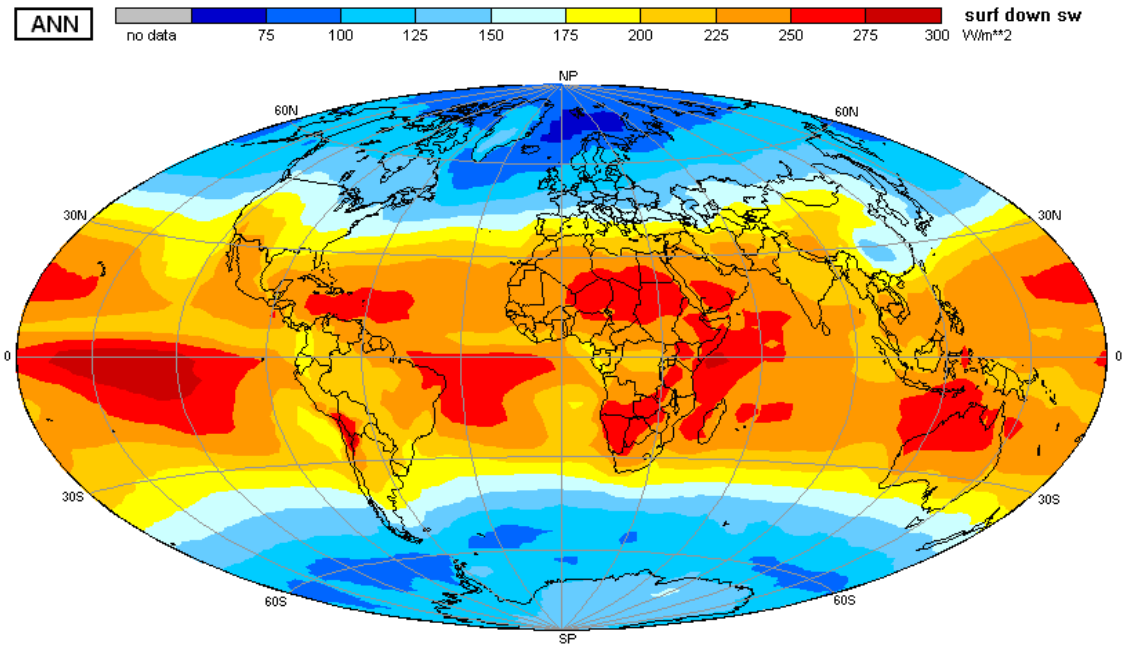

Fig. 4.3.4.3a Annual average of the downward solar radiation at ground during the period 1991 to 1995 in Wm^{-2}. Prime modifiers of these fields are the mean solar height over each area and the persistence and thickness of cloud fields. Note the low amounts over southern China. Extreme small values are obtained over the northernmost Atlantic Ocean. Highest and lowest values: 286 and 60 Wm^{-2}; global average: 189 Wm^{-2}. The values are possibly too high by about 5 to 10 Wm^{-2} as preliminary comparisons with ground-based measurements have shown.

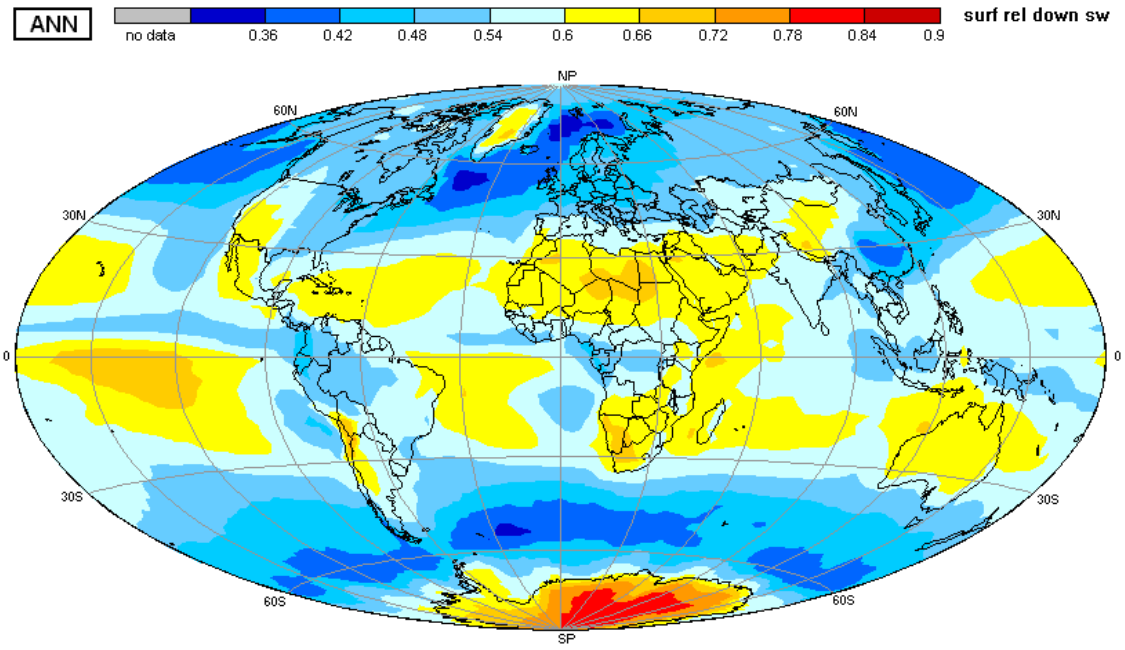

Fig. 4.3.4.3b Annual average of the relative values of the downward solar radiation at ground, related to the incident radiation at the top of the atmosphere during the period 1991 to 1995. These values are equivalent to a mean atmospheric transmittance of the atmosphere for solar radiation. This presentation enhances the role of cloud fields and of the topographic height of various continental surfaces. Highest and lowest values: 0.82 and 0.33; global average: 0.55. Such relative information is very important for initial planning of environmental projects.

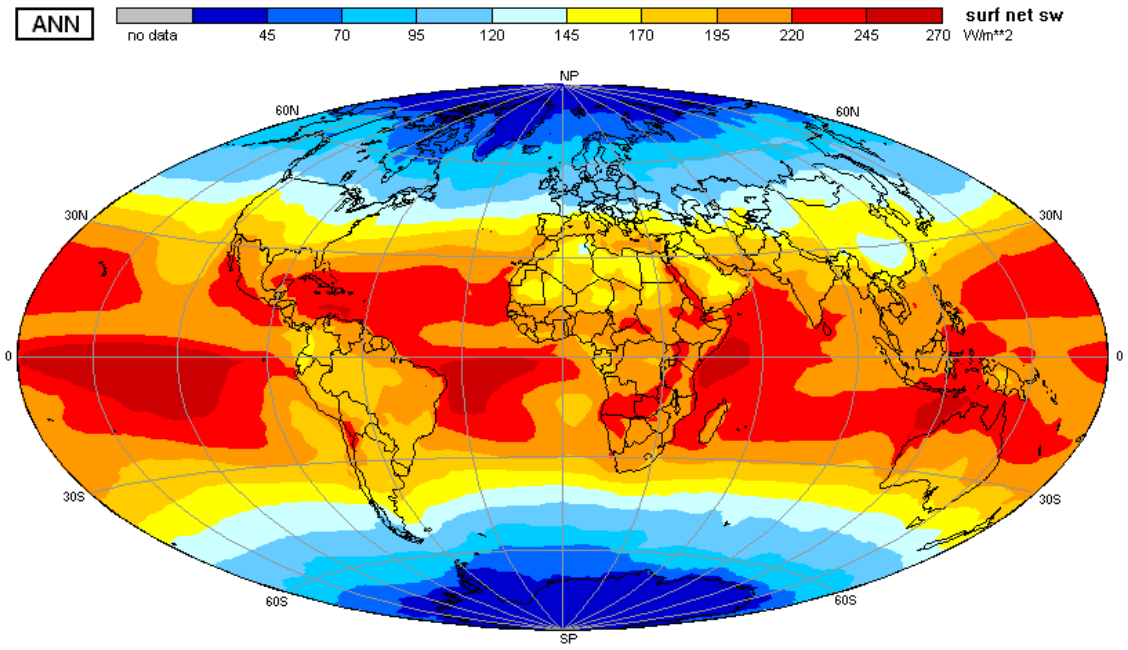

Fig. 4.3.4.4 Annual average of the solar net radiation at ground, which is the downward solar minus reflected fraction of it during the period 1991 to 1995, in Wm^{-2}. This map identifies the regions with low surface albedo and low cloudiness to gain highest amounts of incoming radiation. Highest and lowest values: 270 and 22 Wm^{-2} ; global average: 165 Wm^{-2}.

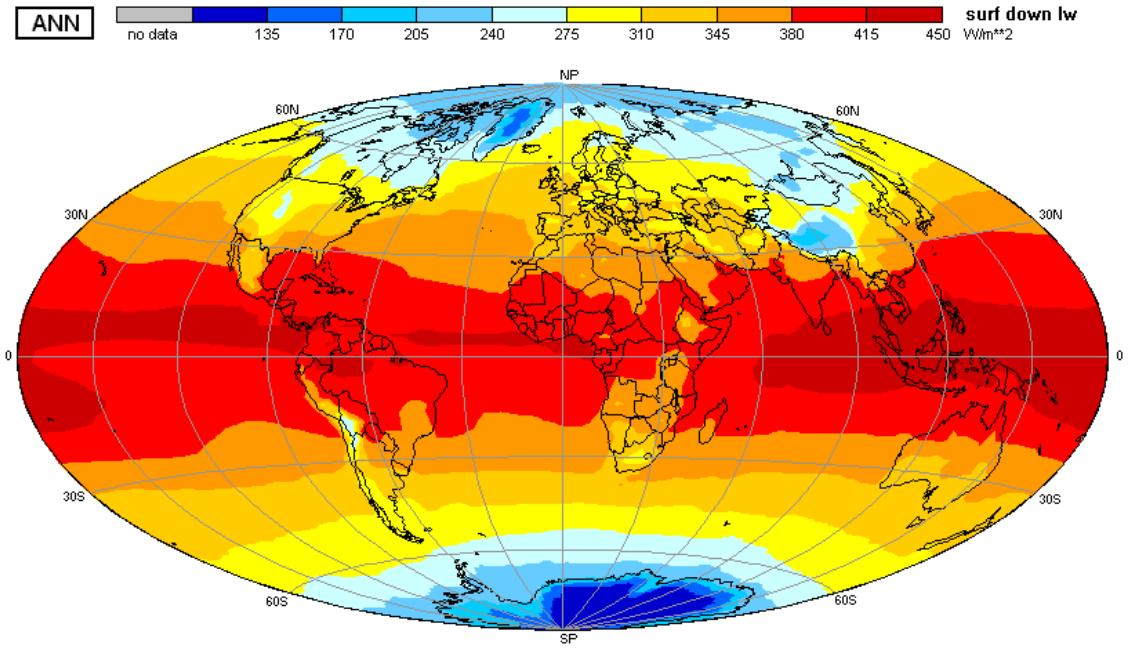

Fig. 4.3.4.5 Annual average of the downward terrestrial (atmospheric) radiation at ground during the period 1991 to 1995, in Wm^{-2}. These fields are dominated by the temperature and water vapor content of the lower troposphere and at higher latitudes also by cloud base heights. Highest and lowest values: 431 and 101 Wm^{-2}; global average: 343 Wm^{-2}.

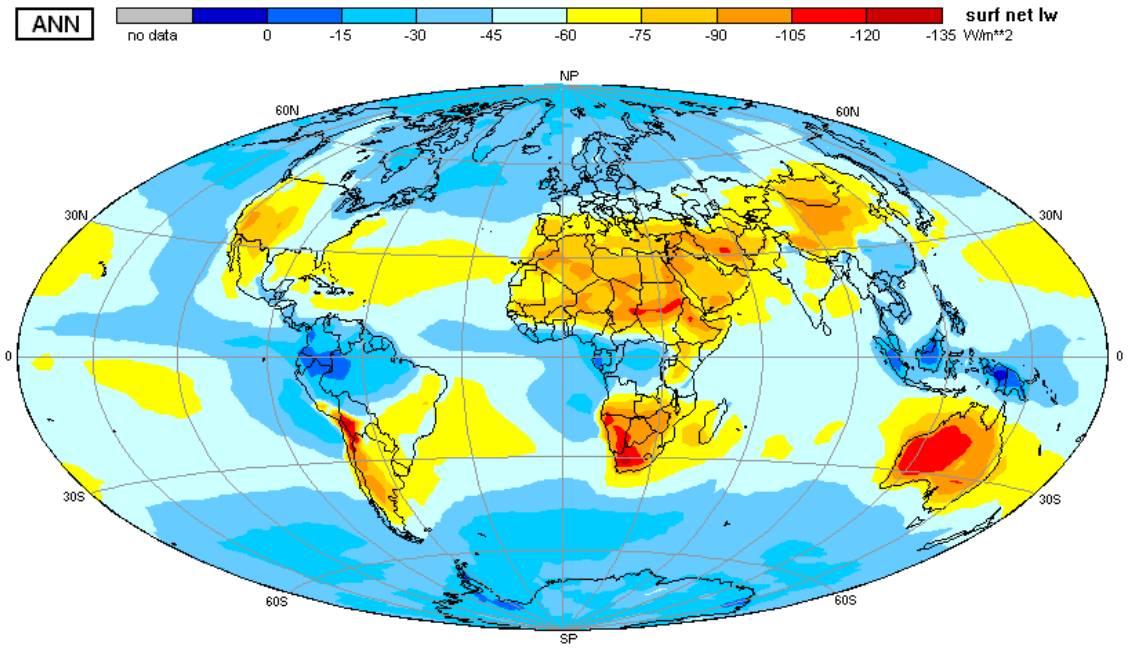

Fig. 4.3.4.6 Annual average of the net fluxes of terrestrial radiation at ground, computed from the difference between the downward atmospheric and the upward surface heat radiation during the period 1991 to 1995, in Wm^{-2}. All values are negative indicating, that in the average the ground heats the atmosphere above. Highest and lowest values are –10 and –134 Wm^{-2}; global average : – 50 Wm^{-2}.

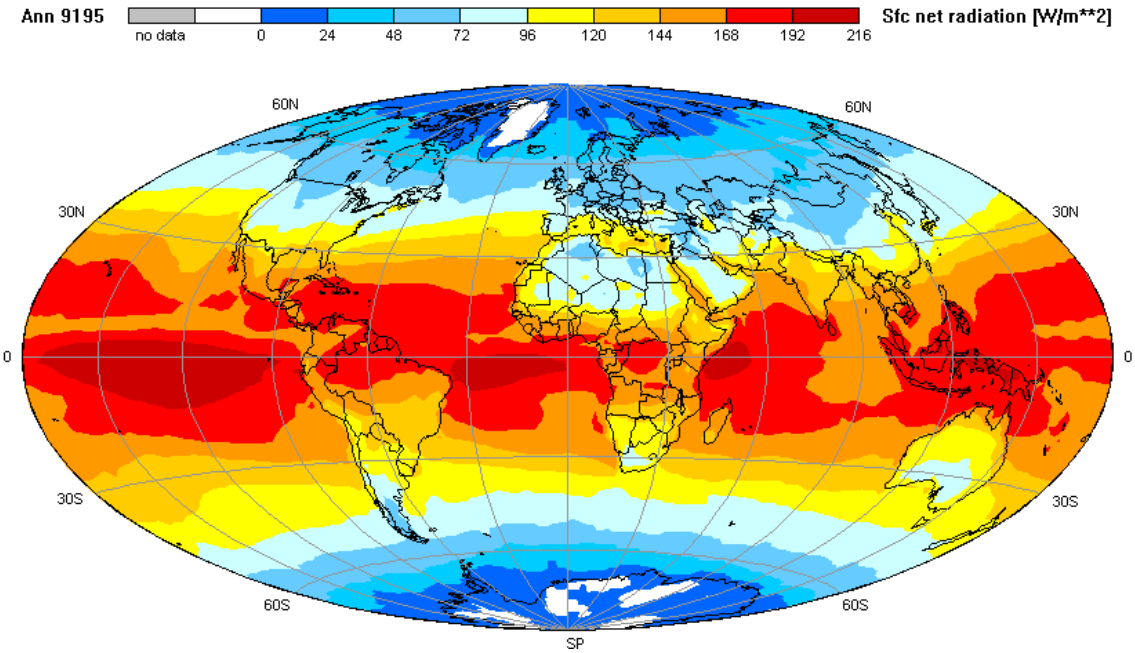

Fig. 4.3.4.7 Annual average of the total net radiation (or of the radiation budget) at the surface during the period 1991 to 1995, in Wm^{-2}. All values, with a few exceptions over Greenland and Antarctica, are positive indicating, that the Earth's surface is everywhere heated by radiation. The small negative white areas are very close to zero. They are possibly caused by errors in both components over those regions, due to inaccurate cloud identification over those regions. Highest and lowest values: + 211 and –16 Wm^{-2}; global average: +116 Wm^{-2}.

4.3.4.3 Effects of clouds on the surface radiation budget

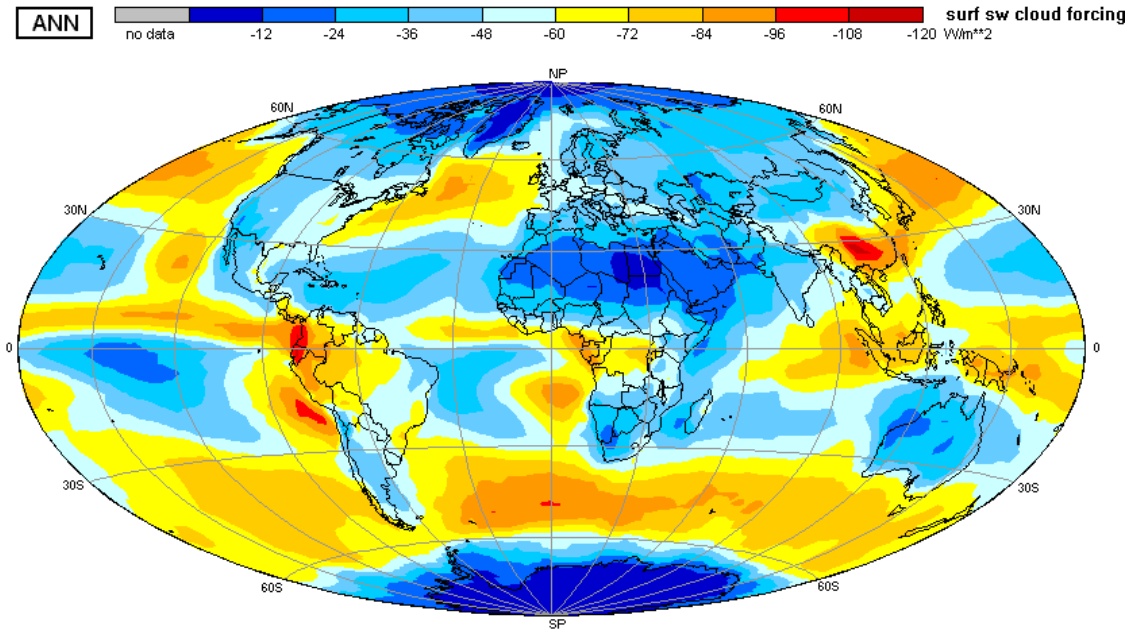

Fig. 4.3.4.8 Annual average of the effects of clouds during the period 1991 to 1995, **in Wm^{-2}**, **on the solar net radiation** at ground, computed as the difference between the respective mean map (Fig. 4.3.4.4) and a map for cloud free skies. **Clouds generally reduce** the downward fluxes of solar radiation. Largest differences occur over the tropics and over extra-tropical storm track regions. Highest and lowest values are −2 and −114 Wm^{-2}; global average: −52 Wm^{-2}. The largest reductions of solar occur over Southern China and the northwestern edge of South America.

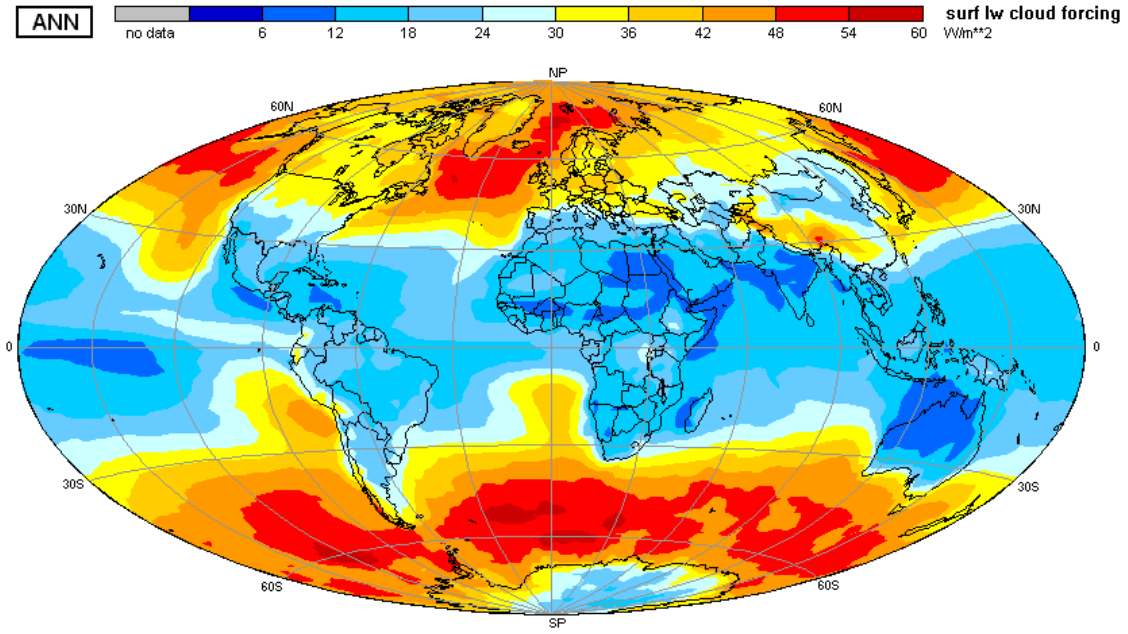

Fig. 4.3.4.9 Annual average of the effects of clouds during the period 1991 to 1995, **in Wm^{-2}**, **on the terrestrial net radiation** at ground computed as the difference between the mean map in Fig. 4.3.4.6 and a map for clear skies. This effect is generally positive over all areas, since **clouds enhance** the downward atmospheric radiation. Over continents these values are less reliable since for this analysis only scarce information on the real surface temperature was available. Highest and lowest values are 57 and 6 Wm^{-2}; global average: + 30 Wm^{-2}.

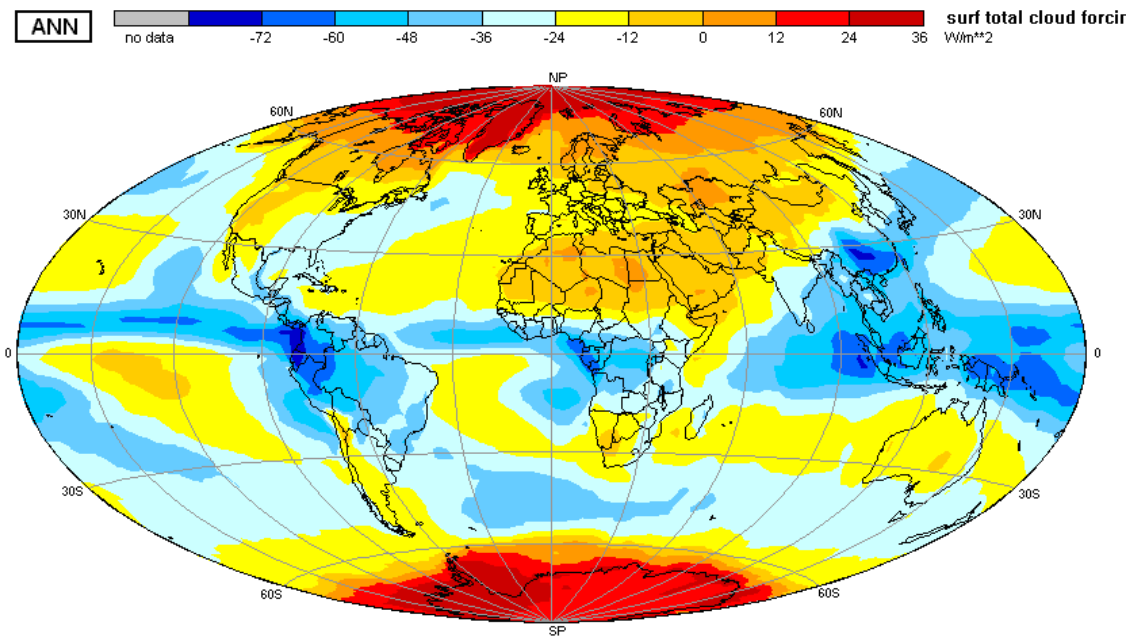

Fig. 4.3.4.10 Annual average of the effect of clouds on the net radiation (or radiation budget) at ground (in Wm^{-2}) computed as the difference between the mean map in Fig. 4.3.4.7 and a map for clear skies or from the sum of the quantities in Figs. 4.3.4.8 and 9. Over most areas clouds reduce the gain of radiative energy of the ground. Highest and lowest values are +35 and –85 Wm^{-2}; global average: –23 Wm^{-2}. Areas of pronounced (more than 20 Wm^{-2}) heating occur over both Polar Regions, where the identification of clouds, however, is quite difficult.

In general clouds alter the amount, spectrum and angular distribution of solar radiation reducing its total amount. They add to the up- and downward atmospheric radiation.

In the two Figs. 4.3.4.11 and 12 we summarize zonal averages of annual and seasonal values, which help to understand better the role of clouds in the radiation budget components at both boundaries of the atmosphere.

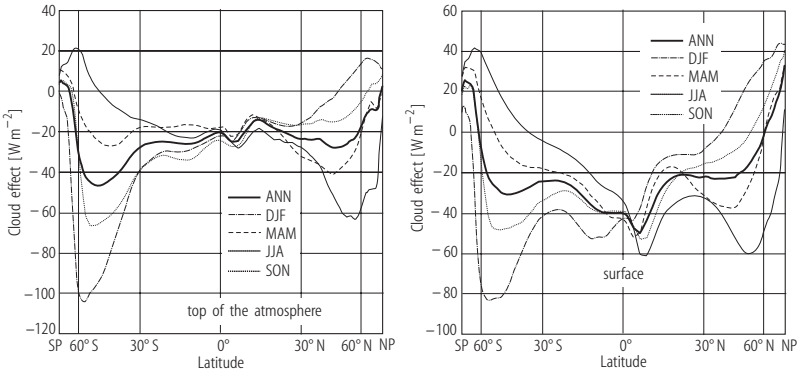

Fig. 4.3.4.11 Zonal annual and seasonal averages of cloud effects on the net radiation budgets at the top of the atmosphere (TOA, left panel) and the surface (right panel). These curves show generally a "heating" of the climate system and the surface, respectively, over the winter hemisphere, poleward of about 35° to 40° latitude. Strongest cooling by clouds is found between 40° and 60° latitude during the respective summer seasons.

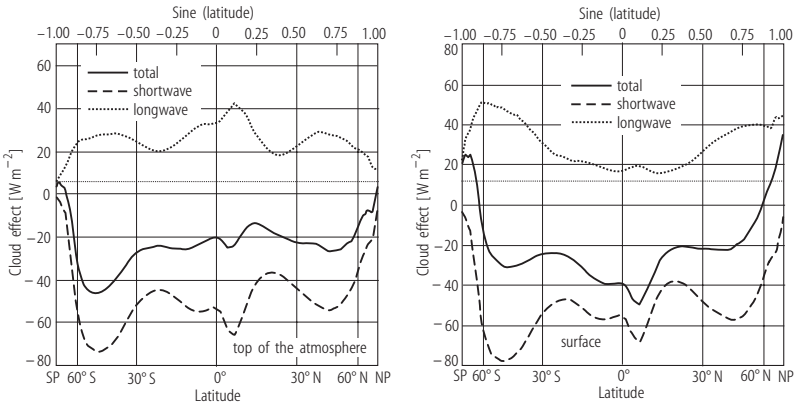

Fig. 4.3.4.12 Zonal annual averages of cloud effects on the solar, terrestrial and net radiation budgets at the top of the atmosphere (TOA, left panel) and at the surface (right panel). These zonal averages emphasize the "cooling" or "heating" effects of clouds in the solar and infrared spectral regions. Comparison of the curves in the left panel with those in Fig. 4.3.3.6 shows quite similar values.

4.3.4.4 Effective albedo and emission temperatures of the surface

In addition to the results shown above we present here maps of the effective surface albedo and the effective emission temperatures at the surface, which we derived from the difference between the net and downward long-wave radiation at ground. The global annual average of the mean emittance of the earth's surface is 0.975. Respective seasonal averages are given in the next section. In the Southern Sahara and in NW Australia emission temperatures higher than +40 °C are obtained. Note the "cold spot" over Tibet. The Antarctic Plateau is colder than –40 °C.

Figs. 4.3.4.13 and 4.3.4.14, see next page.

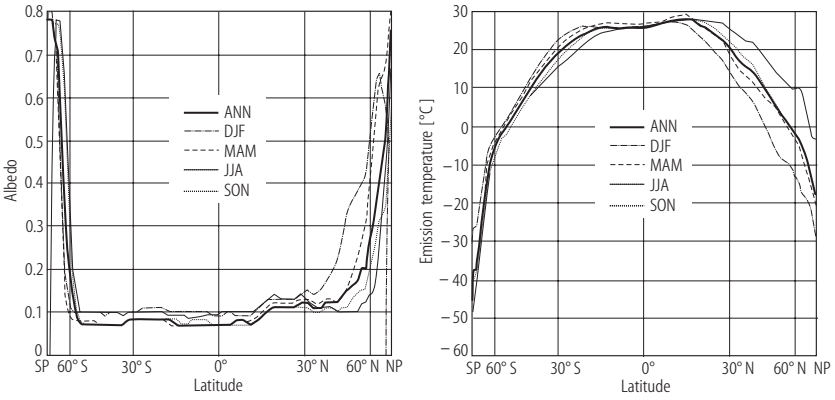

Fig. 4.3.4.15 Zonal means of seasonal averages of the effective albedo and emission temperature of the Earth's surface.

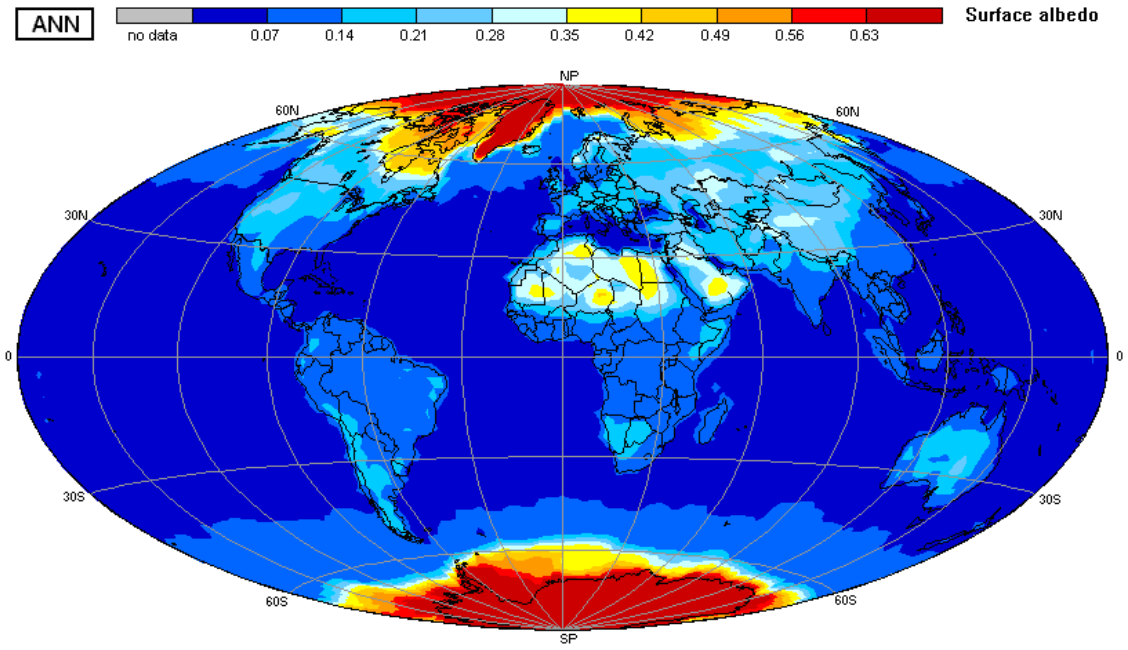

Fig. 4.3.4.13 Annual average of the effective values of the surface albedo of the earth for solar radiation during the period 1991 to 1995, in Wm^{-2}. These fields result from various assumptions on the real albedo and their increase with increasing zenith angle of the Sun, and on operational reports of snow and ice cover. Lowest values over the ocean for Sun at zenith are 0.06 and highest values over the polar snow and ice fields are 0.7. Highest and lowest values: 0.80 and 0.07; global average: 0.13. The albedo of the water was modeled with some dependence on the solar zenith angle, cloud amount and the wind speed.

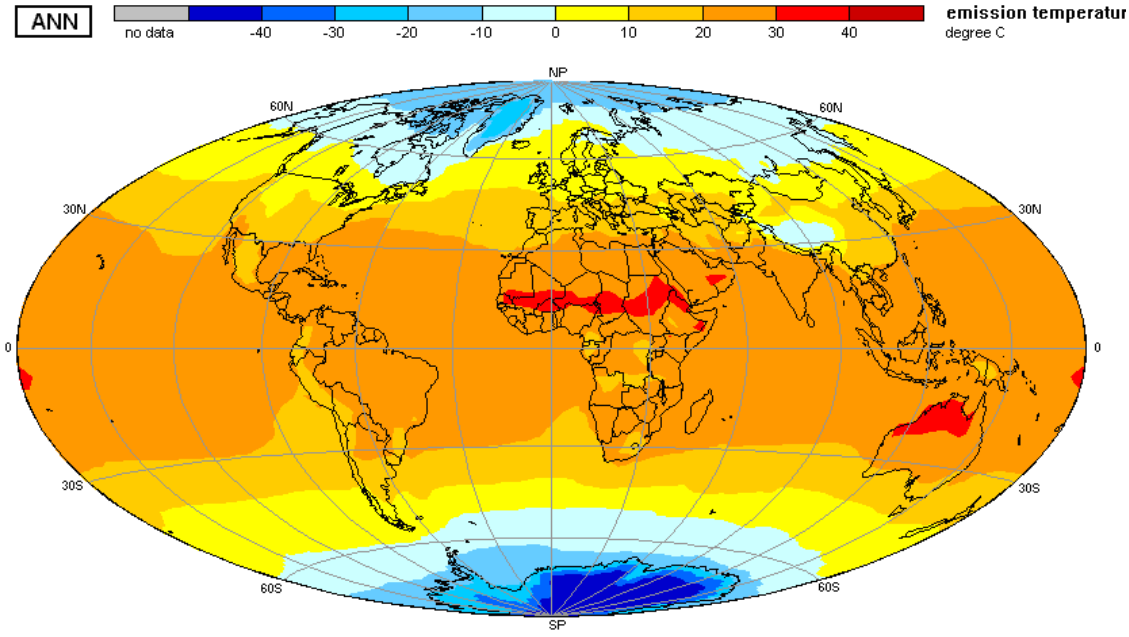

Fig. 4.3.4.14 Annual average of spatial distribution of effective emission temperatures during the period 1991 to 1995. The global average is 15.2 °C. This value agrees with the estimates made by Jones et al. (99Jon) for the temperature of the atmosphere near ground. A mean surface emittance of 0.93 to 0.98 has been assumed throughout the entire procedure, which raises the effective temperatures by about 2.0 K against the real ones. Highest and lowest values are +34 and –56 °C.

In the computational procedure values for the surface albedo are prescribed for each individual area. The seasonal variations, as visible in the zonal averages below (Fig. 4.3.3.15) are primarily due to seasonal variations in sea ice and snow cover. The continents over the Northern Hemisphere dominate the seasonal variability of emission temperatures.

4.3.5 Vertical radiative flux divergence in the atmosphere

We define here the vertical (columnar) radiative flux divergence as the difference between the net radiant flux densities at the top of the atmosphere and at ground. Thus **positive** values describe a gain (heating by convergence) of radiant energy and **negative** values a loss (cooling by divergence) by the atmosphere, where we consider again the Earth as a planet. This change of sign in the classical definition of the divergence is forced by our view of the Earth (or formally: negative altitude).

4.3.5.1 Global fields

Largest amounts of solar radiation of more than 80 Wm^{-2} remain in the tropical and subtropical atmosphere. Interestingly maxima of more than 96 Wm^{-2} can be observed over the southern part of the Arabian Peninsula and over the Gulf of Somalia. Both areas are usually poorly covered by clouds, thus these maxima are caused by absorption in lower tropospheric water vapor. The pronounced minima over Greenland and the Antarctic Plateau reflect the extremely low water vapor content of the atmosphere over those cold and high regions.

Typical vertical profiles of the total atmospheric radiative cooling have already been shown in Fig. 4.3.1.2. They indicate that the long-wave cooling to space dominates the heating by absorption of solar radiation within the troposphere. Therefore, all values total radiative flux divergence, are negative, indicating that over all areas radiant energy is lost. Highest losses occur over the low marine stratocumulus fields over the eastern portions of Pacific and Atlantic Ocean. Over the continents the losses are generally much smaller than over Oceans. The different effects of high and low clouds in the solar and terrestrial spectral regions are delineated in the maps for the divergences of solar short-wave and terrestrial long-wave radiation which are shown in Figs. 4.3.5.1 and 4.3.5.2. These maps also show the different emissions from areas with high and low water contents in the lower troposphere.

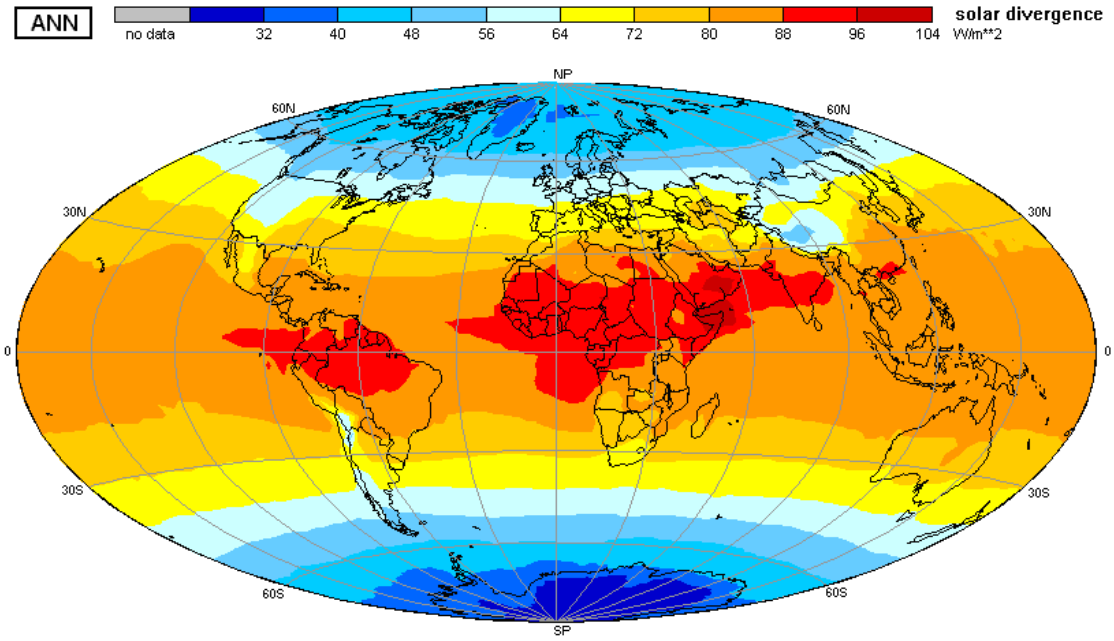

Fig 4.3.5.1 Annual average of the divergence of solar radiation during the period 1991 to 1995, **in Wm^{-2}**, as absorbed in the atmosphere (computed as difference between solar net radiation at the top and bottom of the atmosphere. Strongest absorption occurs in the tropics and subtropics with a maximum over and south of the Arabian Peninsula. The minimum over Tibet reflects the high elevation of this plateau. Highest and lowest values are 104 and 22 Wm^{-2}. The global average is 70 Wm^{-2}.

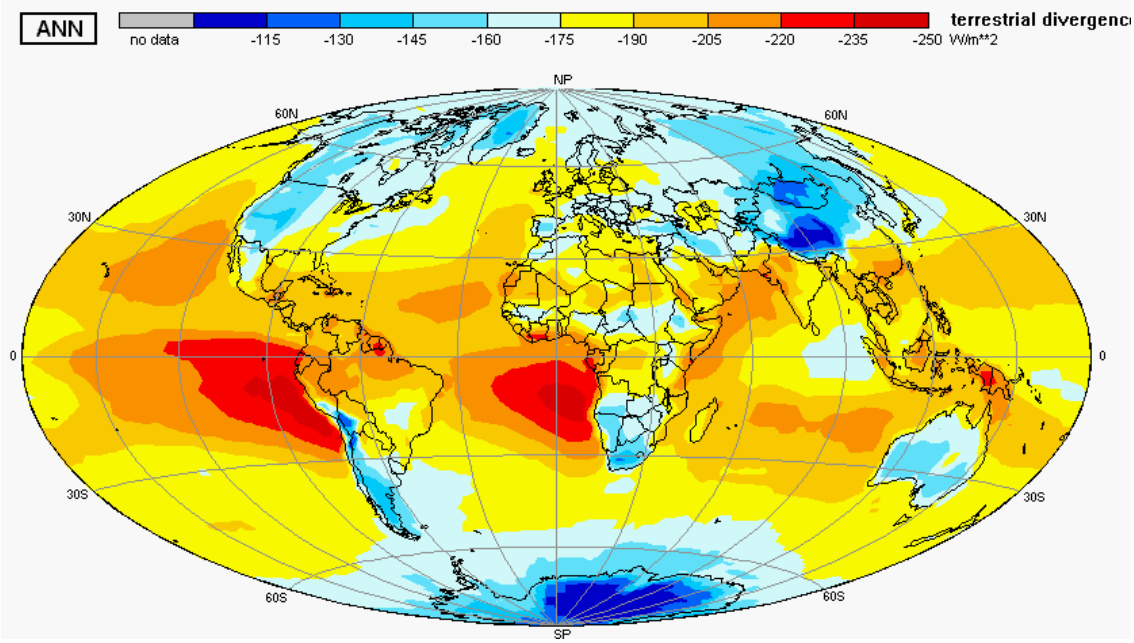

Fig. 4.3.5.2 Annual average of the divergence of terrestrial radiation in the atmosphere during the period 1991 to 1995, **in Wm^{-2},** computed as the difference between the **net fluxes** of terrestrial radiation at the top and bottom of the atmosphere. This map shows essentially the net loss of heat radiation by the atmosphere to space. Highest amounts are found over the persistent low and therefore warm fields of marine stratocumulus, while much lower amounts are found over higher elevated continental surfaces, drier semi-deserts, and of regions with persistent high level clouds in the tropics. Highest and lowest values are –96 and –242 Wm^{-2}. The global average is –184 Wm^{-2}.

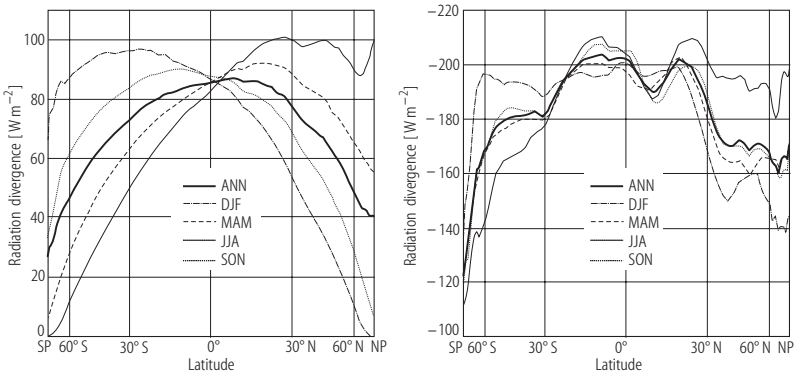

Fig. 4.3.5.3 Zonal averages of the solar (left) and terrestrial (right) radiant flux divergence in the atmosphere during all seasons. The solar radiation is absorbed (positive values) while in the net effect more longwave radiant energy is lost to space than absorbed in the total atmosphere.

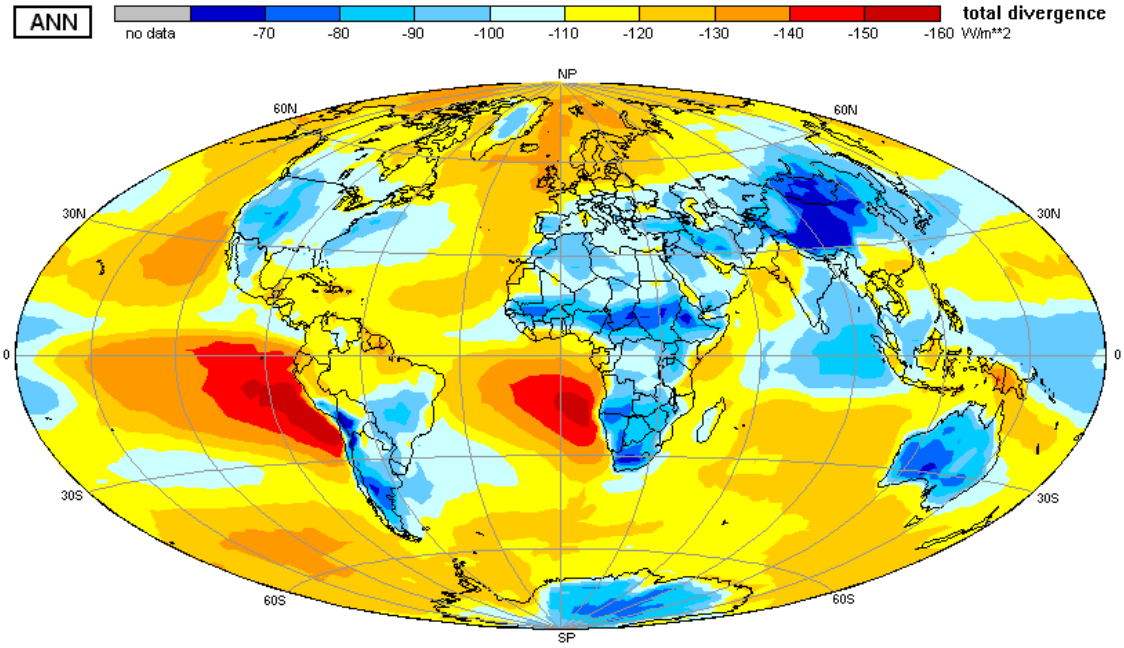

Fig. 4.3.5.4 Annual average of the total radiant energy flux divergence in Wm^{-2} during the period 1991 to 1995, as computed from differences of the annual means of the net radiation at the TOA and at ground. Negative values mean loss of radiative energy to space. Highest and lowest values are −51 and −158 Wm^{-2}**.** The global average is −113 Wm^{-2}. The two major maxima of radiative cooling to space occur over the fields of low and often optically thin clouds over the southern subtropical Pacific and Atlantic Oceans.

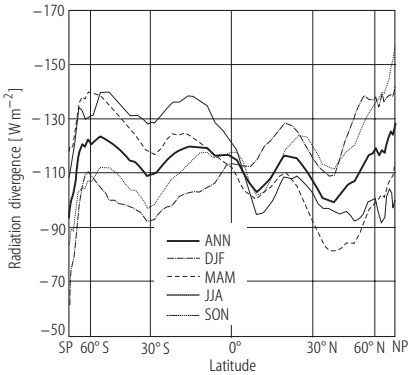

Fig. 4.3.5.5 Zonal averages of the total radiant flux divergence in the atmosphere during all seasons. These graphs are obtained for all seasons and for the annual average.

4.3.5.2 Effect of clouds on the vertical flux divergence

The ISCCP result allow for the first time estimates of the influence of cloud fields on the fields of the radiant flux divergence. This can be done simply subtracting the respective maps (sections 4.3.3.2 and 4.3.4.3 of this chapter) at the ground from that at the top of the atmosphere. We show only the global maps below:

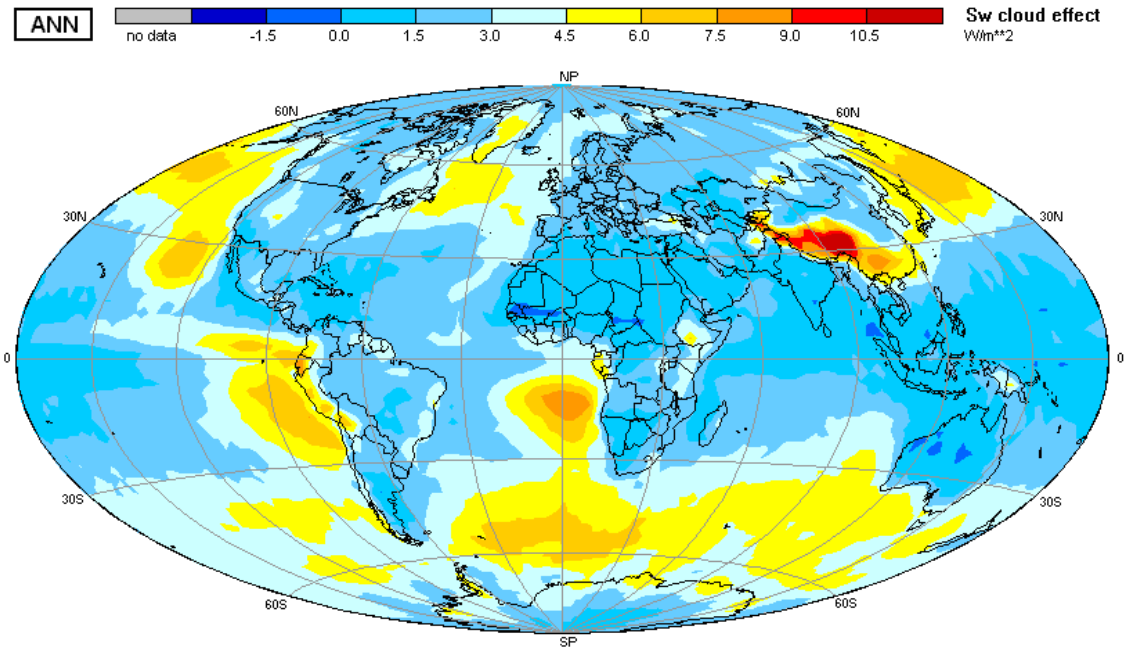

Fig. 4.3.5.6 Annual average of the effects of clouds on the vertical divergence of solar radiant energy (in Wm^{-2}) during the period 1991 to 1995. This map is the difference between the respective maps for cloud effects at TOA and at ground. It also can be obtained from the difference between the respective maps of cloud effects on the solar budgets at TOA and at ground. Very small negative values are observed at a few spots. They might be caused by errors in cloud identification for the upward radiation. The global average is 3 Wm^{-2}; highest value 12 Wm^{-2}, lowest value –2 Wm^{-2}. This range is surprisingly small, possibly due to an overestimation of downward solar radiation in all ISCCP data (see also error discussion in 4.3.6).

The absorption of solar radiation in the cloudy atmosphere in the tropics and subtropics seems to be very small apparently due to the overwhelming high absorption by atmospheric water vapor at clear skies, which is then reduced in the presence of clouds. The two maxima over Tibet and southern China need further explanation, where the first one seems to be due to the high elevation of this area. The higher absorption over the marine stratocumulus and the major storm tracks over the oceans appears realistic, while the relative high values over Greenland and the even "negative absorption" occurring as darker blue spots over Africa, Australia and elsewhere seem to reflect the uncertainties in cloud identifications for this estimate. The reader, however, should take these results as a first orientation towards more accurate radiation climatology. The generally small values of this quantity (see also the zonal averages in Fig. 4.3.5.9) seem to be justified by the fact, that in presence of clouds the otherwise quite effective absorption of solar radiation by the lower tropospheric water vapor is almost completely cut off. The absorption inside of clouds is indeed not very high although earlier airborne measurements resulted in often high values. But these findings could be partly explained by instrumental deficiencies and by the cloud structures (see summary by 03Li). On the other side, the estimates of the solar radiation budget at the surface might be too high by 5 to 10 Wm^{-2} as comparisons with station values of the downward solar radiation have shown.

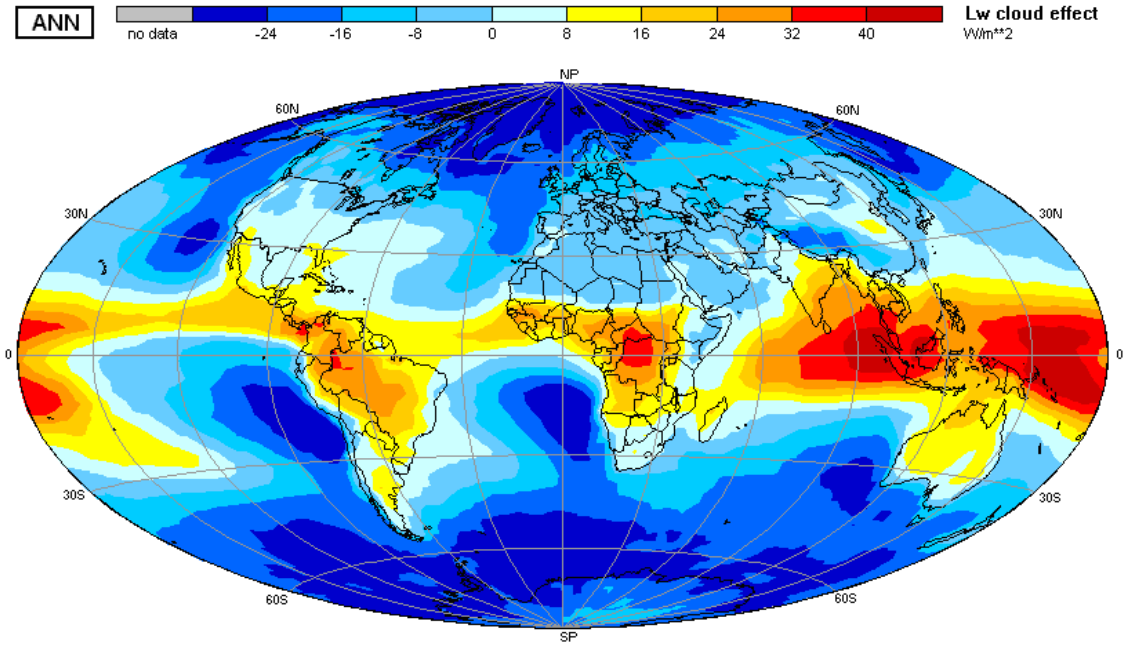

Fig. 4.3.5.7 Annual average of the effects of clouds on the vertical divergence of terrestrial radiant energy (in Wm^{-2}) during for the period 1991 to 1995. This map is the difference between the respective maps for cloud effects at TOA and at ground. Over all positive areas clouds enhance the long-wave divergence, due to their higher tops. Over all negative areas they reduce it, since they are mostly low. The drastic reduction at higher latitudes is primarily caused by stronger cloud effects on downward atmospheric radiation, since much less than in the tropics water vapor is present in the lower troposphere. The global average is –4 Wm^{-2}; highest and lowest values: + 46 Wm^{-2}, –30 Wm^{-2}.

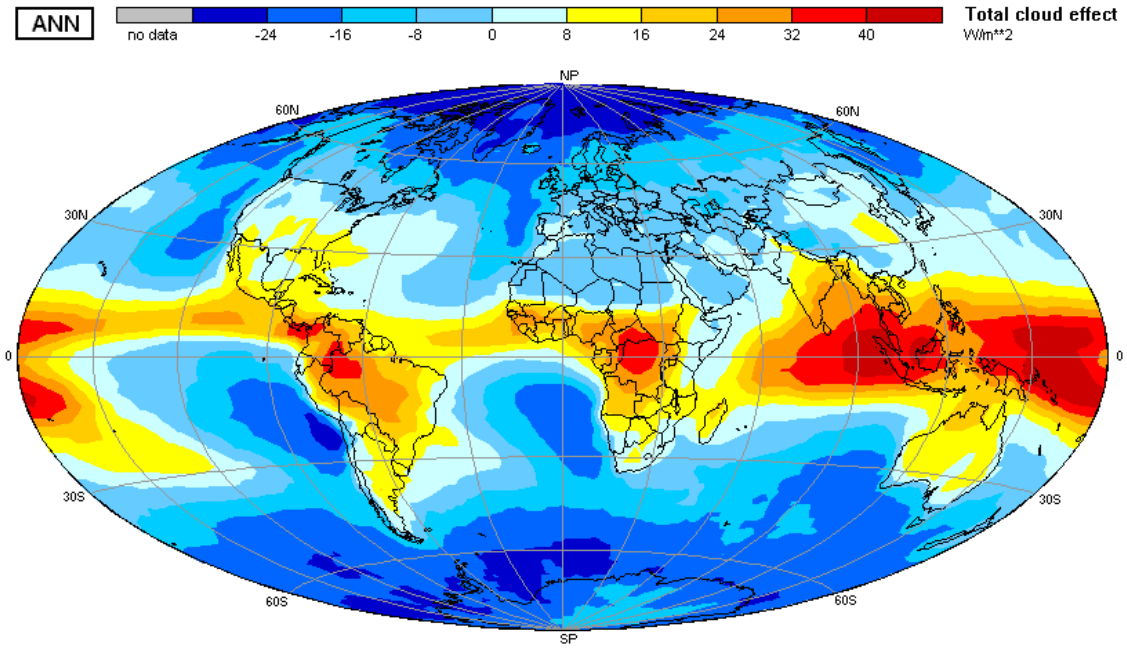

Fig. 4.3.5.8 Annual average of the effects of clouds on the vertical divergence of total (solar and terrestrial) radiant energy (in Wm^{-2}) during the period 1991 to 1995. This map is the difference between the respective maps for cloud effects at TOA and at ground. The effect of clouds on the long-wave divergence dominates partly its pattern on the total radiant divergence. It is enhanced in the tropics over areas with often high convection, but reduced over lower marine stratocumulus. The global average is –1 Wm^{-2}; highest value: +45 Wm^{-2}, lowest value: –28 Wm^{-2}.

In the figure below we show the zonal averages to emphasize the overwhelming effect of clouds on the divergence of terrestrial (infrared) radiation, while the divergence in the solar region of the spectrum is relatively small and nearly constant. In the latter case two major effects tend to cancel. These are the relatively weak absorption of solar radiation in cloud fields, which is adding to the absorption, and the reduction of absorption in the lower tropospheric water vapor below the cloud fields, which is in particular very high at lower latitude regions.

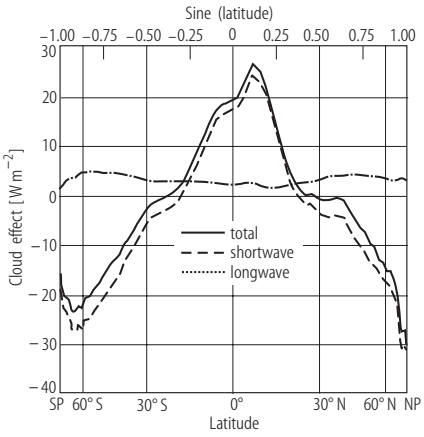

Fig. 4.3.5.9 Mean annual effect of clouds on the total radiant energy flux divergence in the atmosphere. Positive values indicate that clouds contribute to the heating of the atmosphere. Clouds reduce the absorption of solar radiation below their bottoms and may slightly increase the absorption of radiant energy in the stratospheric ozone layer. The cloud effect in the infrared is due to partly compensating effects of emission from cloud tops and cloud bottoms at different altitudes and also the emission of lower atmospheric water vapor to ground.

4.3.6 The global annual budget and a preliminary error discussion

There have almost no error estimates made yet of the ISCCP radiation budget data set, except those by (95Zha), which are summarized in Table 4.3.6.2. There is indeed a wide range of error sources: In the identification of clouds and of their optical thickness, in all input data used for such calculations and also in the radiative transfer code.

Most possible error analysis is possible for the radiation fields at TOA by their comparison with same fields of the same period, but computed from other data sources or direct measurement. This kind of intercomparison cannot provide absolute errors but it can identify regions of systematic deviations between both data sets and set limits for ranges of uncertainty. Some preliminary results, which were provided by B. Carlson and P. Stackhouse (both with NASA, USA) as personal communications, showed, that over most regions of the Earth these results agreed within about ±5 to 10 Wm^{-2} for both the reflected solar and the emitted terrestrial radiation. There are direct comparisons possible with airborne measurements of upward fluxes only in rare cases of complete cloud-free and of unique cloud fields over large areas, as viewed from altitude of about 15 km. However such measurements have an uncertainty range of the same amplitude as given above.

Similar comparisons can also be done with the fields of downward solar and terrestrial radiation at ground, where additional support is possible by data from station networks. Comparisons with several individual stations (M. Wild, private comm., 2003) indicate a small overestimate of solar radiation budget at the surface by about 5 to 10 Wm^{-2}. These are reproduced in Fig. 4.3.6.1. But, it should never be overlooked, that even the "most accurate" surface based direct measurements of downward solar and atmospheric radiation are not better than ±1 -2% of a daily mean value! Further, even the best station is more or less representative for a smaller area around due to inhomogeneities in the atmosphere (primarily caused by clouds).

In Fig. 4.3.6.2 are shown similar comparisons between station data and ISCCP results for the downward terrestrial radiation. These show much larger scattering, which are partly due to the fact, that the measurements of most individual stations are not representative for the spatial domain of the ISCCP results.

The relative error range for annual averages of all radiation fluxes at TOA is estimated for the global averages in Table 4.3.6.1 to be about ±2 - 4% and about ±7 to 10 % at ground with the basic assumption, that the error of regional averages (e.g. for an area of 2.5×2.5 degrees) contains both a bias and a fluctuation, where the latter is then by averaging over the entire globe and over a full year reduced considerably. Thus these error values should be considered to be ranges of uncertainty, which immediately become larger, when two such values are subtracted.

Further important error sources are: systematic uncertainties inherent to the retrieval technique itself, spatial representativeness of validation data (e.g.: ground based measurements), diurnal sampling, cloud identification, variability of atmospheric aerosol content in particular over regions of biomass burning, use of additional data on atmospheric and surface properties (e.g. temperature of lower troposphere or surface temperature over continents), angular dependence of reflected and emitted radiances as seen from the satellite, restricted spectral sensitivity of the operational satellite sensors used to establish the ISCCP radiance data sets. Emittance values for the Earth's surface range between about 0.95 and 0.995.

A small annual imbalance of the net radiation of 3 Wm^{-2} cannot be interpreted as a result of increasing heating due to increase of greenhouse gas concentrations. The seasonal variation of the quantity finds a plausible explanation by non-symmetric distribution of continents over both hemispheres.

	solar	terrestrial
TOA	11 Wm^{-2} (7 Wm^{-2})	–1 Wm^{-2} (4 Wm^{-2})
SFC	10 - 15 Wm^{-2} (10 Wm^{-2})	10 - 15 Wm^{-2} (15 Wm^{-2})
	3 Wm^{-2}	12 Wm^{-2} (20 Wm^{-2})
DIV	20 - 25 Wm^{-2}	10 - 20 Wm^{-2}

Table 4.3.6.1 Estimates of biases and (standard deviation) of regional uncertainty ranges for upward radiation fluxes at TOA and down- and upward radiation fluxes at the surface, made by Zhang and Rossow (95Zha) with regional monthly averages. The estimates for the divergence within the atmosphere are based on these numbers.

Table 4.3.6.2 summarizes the global averages of all radiation budget quantities, which are shown in the maps in the previous sections and in the appendix to this chapter on Radiation in the Climate System. These values are compared to the results of other investigations to demonstrate that still some uncertainties exist. Note the large differences between the downward fluxes estimated by Kiehl and Trenberth (97Kie) and in Fig. 4.3.1.1.

Table 4.3.6.2 Global annual and seasonal averages of all radiation budget components show some deviations between the different data sets. **TOA** means top of the atmosphere. Positive values mean fluxes towards the earth's surface; negative values mean fluxes towards space. The global averages of the net radiation budget at the top of the atmosphere are not "forced" towards radiative equilibrium between Earth and space. All values in Wm^{-2}, except for the albedo. All seasonal variations appear plausible. Error estimates are based on estimates for regional values as given in the literature (97Bis) and on the assumption of very small bias of <3 Wm^{-2} of global averages at TOA and of < 10 Wm^{-2} at ground.

Quantity	annual	DJF	MAM	JJA	SON	[97Kie]	**Fig. 4.3.1.1**	Estimated uncertainty range
Incident solar radiation at TOA	342	352	340	332	334	342	342	± 0.5
Reflected solar radiation at TOA	–106	–112	–105	–101	–108	–107	–102	± 5 - 7
Solar radiation absorbed in the climate system	236	240	235	231	236	235	240	± 5 - 7
Planetary albedo	31 %	32 %	31 %	30 %	32 %	31 %	30 %	± 1-2%
Outgoing terrestrial radiation at TOA	–233	–231	–232	–236	–233	–235	–240	± 3 - 5
Radiation budget at TOA	**+3**	**+9**	**+3**	**–5**	**+3**	**0**	**0**	**± 5 - 7**
Downward solar radiation at ground	189	195	190	180	190	198	169	± 7-10
Net solar radiation at ground	165	169	165	160	167	168	144	± 7-10
Downward terrestrial radiation at ground	343	335	342	351	342	324	345	± 15-20
Net terrestrial radiation at ground	–50	–49	–51	–49	–50	–66	–40	± 15-20
Effective surface albedo and temperatures	13 % 15.2 C	13.3 % 13.7 C	13.3 % 15.5 C	11 % 16.6 C	12.1 % 15.1 C	15 % 14.9 C	15 % 14 C	± 2 % ± 2 K
Total net radiation at ground	115	120	114	111	117	102	104	± 15 - 20
Total atmospheric radiative Flux divergence	–112	–111	–111	–116	–114	–102	–104	± 20
Solar radiative flux divergence in atmosphere	71	71	70	71	69	67	96	± 20
Terrestrial radiative flux divergence in atmosphere	–183	–182	–181	–187	–183	–169	–200	± 20

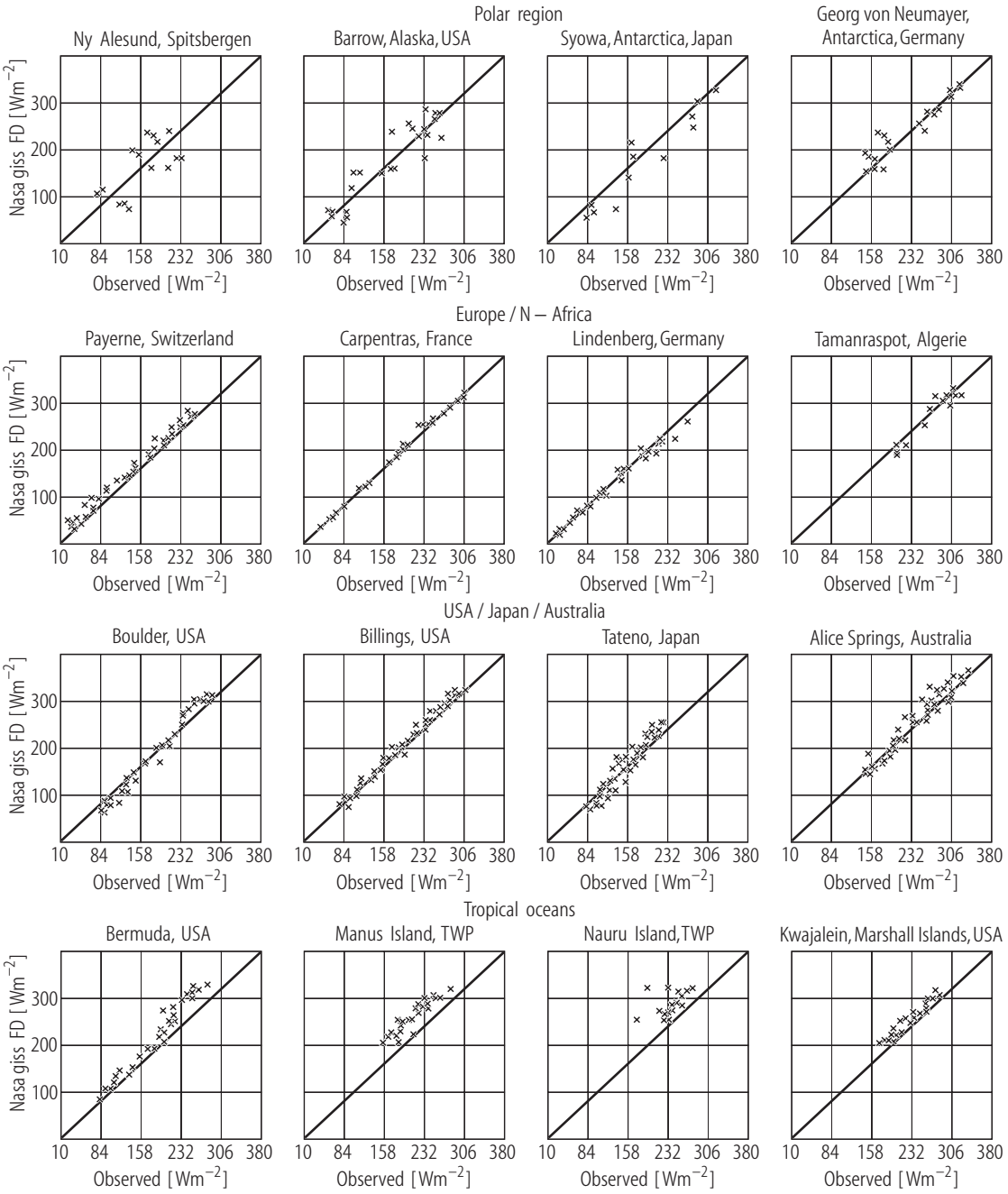

Fig. 4.3.6.1 Comparison of multi-annual averages of the downward flux of solar radiation at ground, estimated from ISCCP data (ordinate) and measured at various stations. The ISCCP procedure seems to overestimate the transmittance of the atmosphere for solar radiation. **Caution:** These are samples for single stations, which are not necessarily representative for areas of 280 km in size. These samples are not all taken during the time period between January 1991 and December 1995. (98Wil and M. Wild, ETH Zürich, personal communication, 2003).

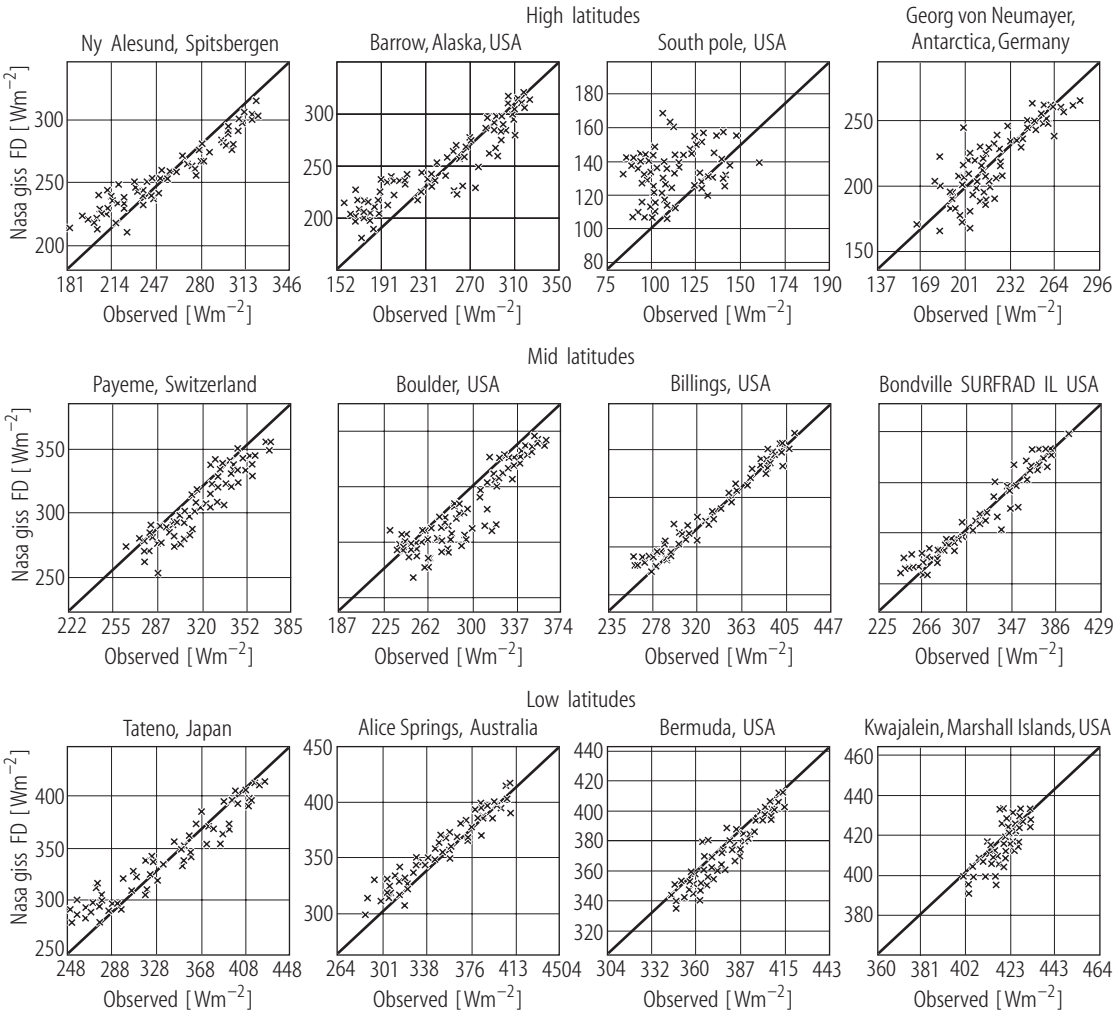

Fig. 4.3.6.2 Comparison of multi-annual averages of the downward flux of terrestrial radiation at ground, estimated from ISCCP data (ordinate) and measured at various stations. The ISCCP procedure seems to overestimate the downward fluxes in particular at smaller value ranges. The large scatter over polar regions is partly due to errors in cloud identification and near-surface air temperatures used as input. **Caution:** These are samples for single stations, which are not necessarily representative for areas of 280 km in size. These samples are not all taken during the time period between January 1991 and December 1995. (98Wil and M. Wild, ETH Zürich, personal communication, 2003).

The values summarized in this Table 4.3.6.3 in connection with the Table before indicate, that clouds cause large changes in the radiation budgets at TOA and at ground. These contributions must further be specified in the vertical domain before conclusions on further feedbacks to the atmospheric circulations can be made. The same holds for the radiative flux divergence within the atmosphere.

Table 4.3.6.3 Global annual and seasonal averages for the period 1991 to 1995 of cloud effects on the radiation budget and on the divergence in the atmosphere are summarized here. Negative values mean at TOA losses to space, or at the surface (SFC) losses into the atmosphere. The annual averages of the cloud effects on budgets at TOA disagree in particular in the longwave radiation from those summarized in Table 4.3.2, possibly due to different methods to identify clouds. This table complements the previous one.

Parameter	ANN	DJF	MAM	JJA	SON
TOA: terrestrial cloud effect	+25	+25	+26	+25	+25
TOA: solar cloud effect	−50	−53	−46	−50	−50
TOA: total cloud effect	−24	−28	−20	−22	−26
SFC: terrestrial cloud effect	+30	+31	+30	+28	+30
SFC: solar cloud effect	−52	−57	−49	−50	−53
SFC: total cloud effect	−23	−26	−20	−21	−24
Cloud effect on terrestrial divergence	−4.3	−5.4	−3.5	−3.2	−5.3
Cloud effect on solar divergence	+3.0	+3.3	+2.7	+2.7	+3.2
Cloud effect on total divergence	−1.3	−2.1	−0.8	−0.5	−2.1

4.4 Photosynthetically Active Radiation (PAR) and Ultraviolet Radiation (UV) at ground

4.4.1 PAR

That portion of the spectrum of solar radiation, which is located between 0.4 and 0.7 μm, is available for photosynthesis and thus is called “Photosynthetically Active Radiation (PAR)”. Irradiance values of the PAR can roughly be estimated from the maps of downward solar radiation using a conversion factor of 0.5. But aerosols, clouds and the angular dependence of attenuation of the direct solar radiation and of the scattering processes forming the diffuse component cause a range of this factor between values of about 0.3 and 0.6, as it has been estimated by Frouin and Pinker (95Fro) – see also Fig. 4.4.1.3.

Their data sets cover the period 1983 to 1993. They are also based on the ISCCP radiance archive. See also: http://www.atmos.umd.edu/~srb/par/webpar.htm). Their earlier results have been compared to some measurements at ground in the Sahel-Zone and found in reasonable agreement.

In the Fig. 4.4.1.1 global maps of a three-year climatology are shown covering the years 1991 to 1993. More data were not available, when this paper was written. The seasonal maps are reproduced in the appendix to this chapter.

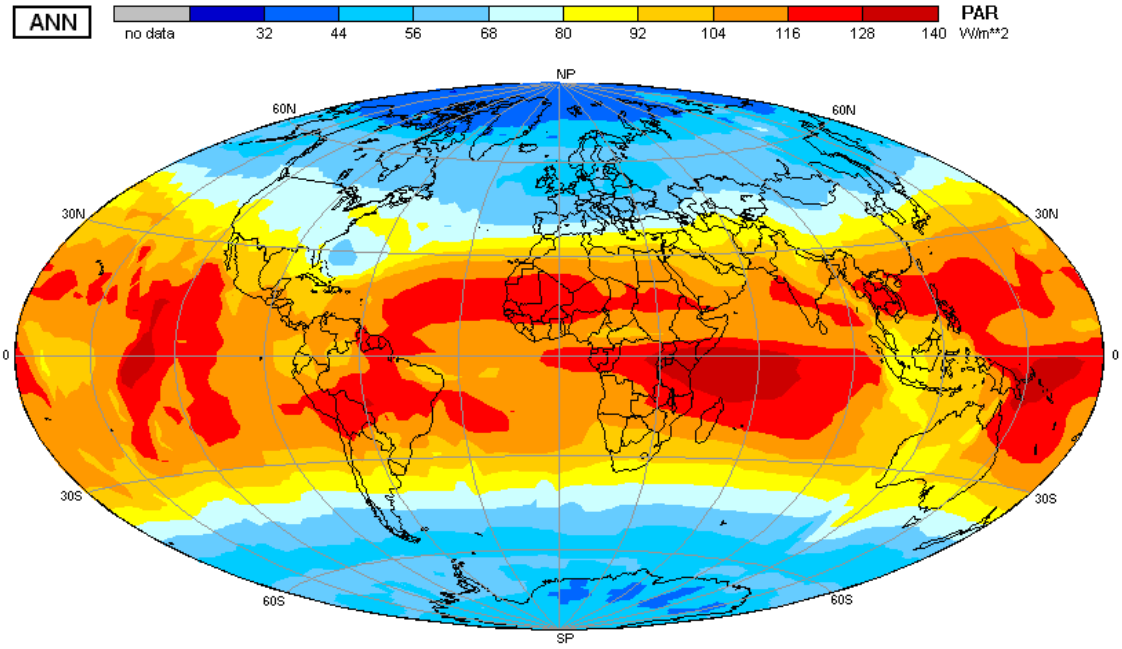

Fig. 4.4.1.1 A three-year climatology (1991 to 1993) of mean annual PAR (in Wm^{-2}), which has been derived from ISCCP radiance data by (95Fro). This pattern is quite similar to that in the map for downward solar radiation. Errors at higher latitude might be higher than at lower latitudes. Due to the lack of a worldwide network of ground stations, an error limit can not be provided. Other definitions of the PAR use the photon flux density ($\mu mol\ s^{-1}\ cm^{-2}$), where 1 Wm^{-2} may correspond to about 4.5 to 5 $\mu mol\ s^{-1}\ cm^{-2}$.

Other estimates have been made with slightly different equations by Bishop and Rossow, (97Bis) and others (97Beh), who concentrated their efforts on the PAR over sea.

There are very strong seasonal variations in the PAR as shown in the figure below.

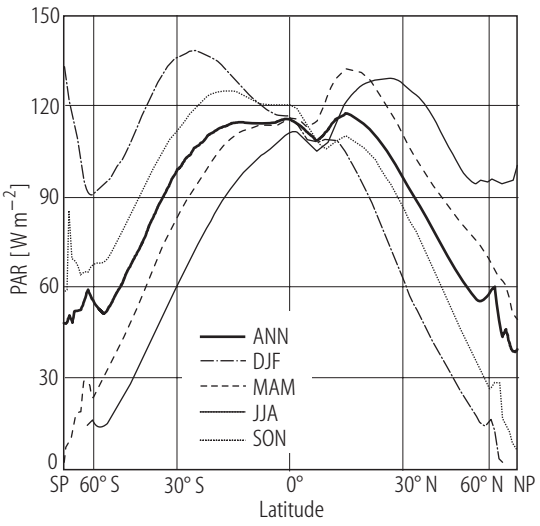

Fig. 4.4.1.2 Zonal annual averages (period: 1991 to 1993) of the PAR. The downward peaks at high southern latitudes are errors. Note the large seasonal variability at extra-tropical latitudes.

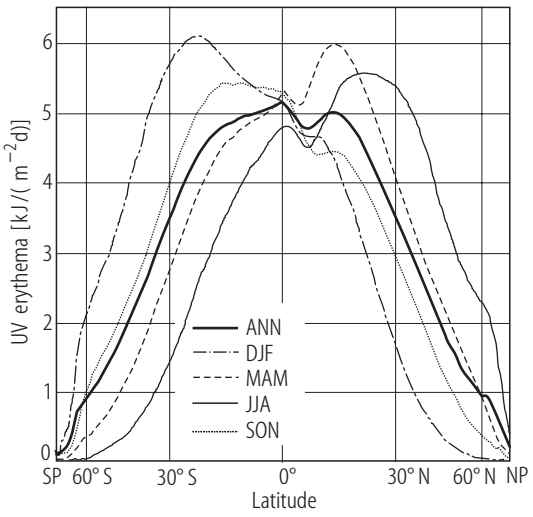

Fig. 4.4.2.2 Zonal averages of seasonal values of the UV erythema doses. Further comments are given above.

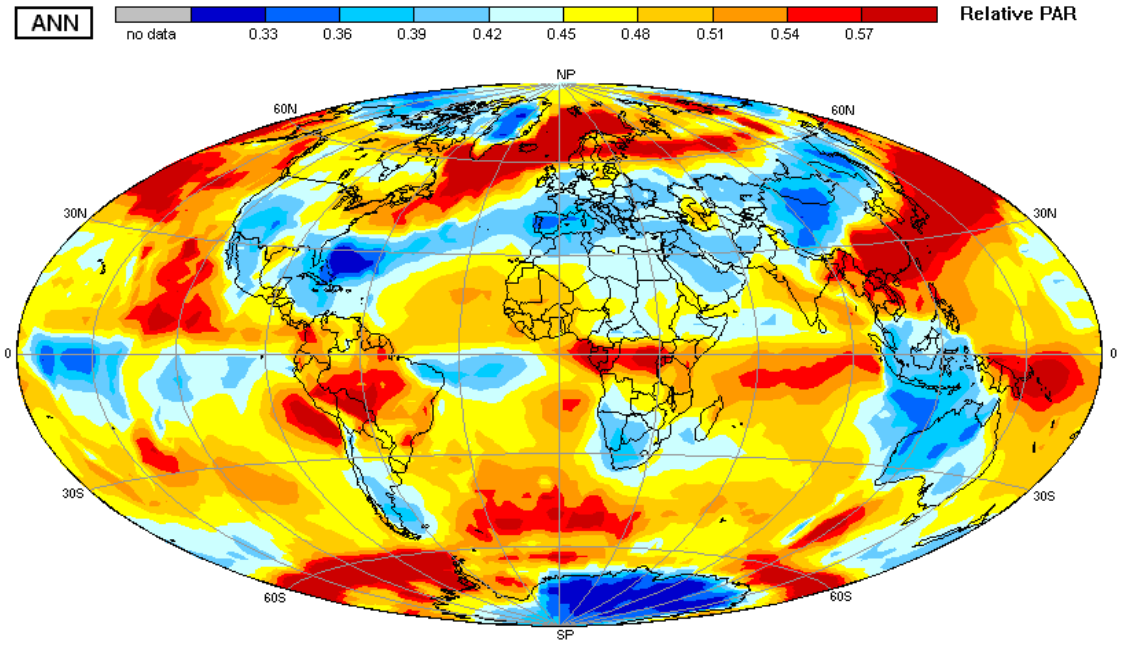

Fig. 4.4.1.3 Ratio between PAR and the downward total solar radiation (relative units). This ratio ranges between values of about 0.3 and 0.6 and seems to depend primarily on the cloud cover, height and thickness. But also aerosol anomalies may play a role in this conversion. We show here this annual map for the convenience of users, who need to estimate PAR from measurements of the global radiation.

4.4.2 Ultraviolet radiation at ground

The solar spectrum in the ultraviolet is divided into 3 parts: UV-C (100-280 nm), UV-B (280-320 nm) and UV-A (320-400 nm). The UV-A accounts for about 6% of the total solar irradiance and amounts to about 7 Wm^{-2} at the surface (93Tak). The UV-C is almost totally absorbed in the layers of the stratosphere and lower mesosphere. The UV-B, corresponding to about only 0.5% of the total solar irradiance, is responsible for most effects of sunlight on the human body and on other members of the biosphere. Its amount is highly dependent on the total amount of ozone in the entire atmosphere. Therefore earlier treatments of the UV-B in the medicine became revitalized by the fact, that at present the total atmospheric ozone is decreasing.

The amount of this radiation reaching the ground is in a complex manner affected by the atmospheric ozone and aerosol content, by the ground albedo in the UV, by clouds (see also 03Mee) and also the altitude of each location. Estimates of this quantity from satellite data or related products derived from satellite data (e.g. the downward solar radiation) are difficult to achieve. Only at a very limited number of stations are measurements done yet. Therefore large uncertainties in these “climatologies” must be accepted. Some national weather services, as also the German Weather Service in Offenbach (http://www.dwd.de), issue now daily forecasts of an UV index to provide some warning for sensitive persons.

The UV erythema doses shown in Fig. 4.4.2.1 should be considered as values of orientation for further application. Their accuracy is too low for trend analyses.

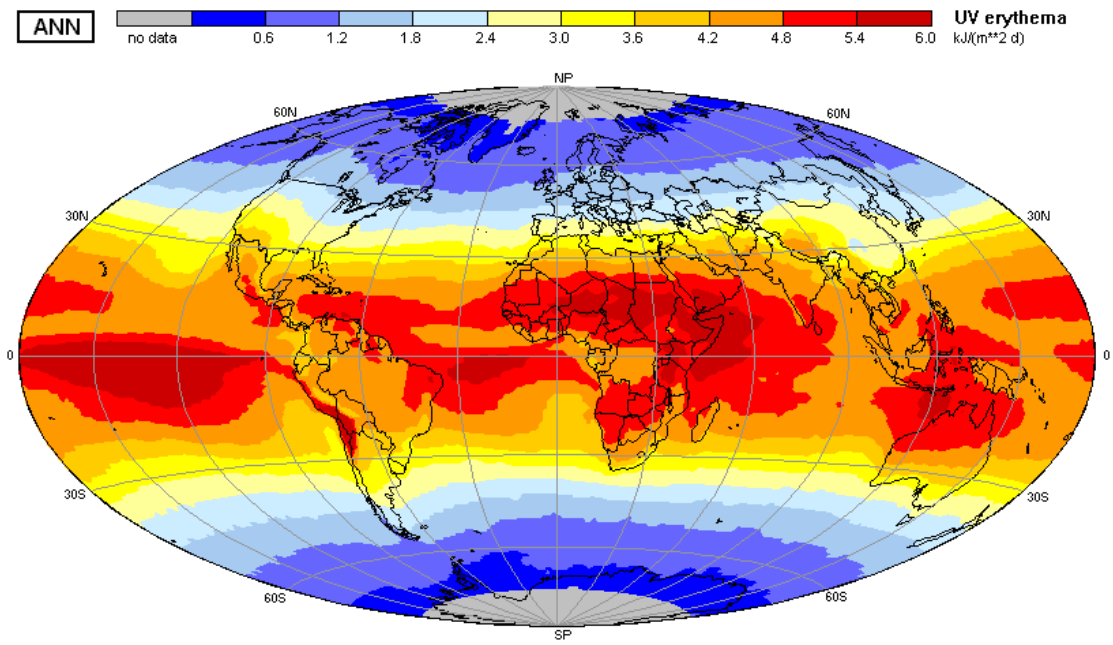

Fig. 4.4.2.1 UV erythema doses (in kJ/m^{2}d) for the period 10/91 to 09/94 have been derived by from data of AVHRR instruments, which are flown on different satellites. The method is not sensitive enough, to reproduce the very small values above both Polar Regions (see internet site: http://www.acd.ucar.edu/TUV).

4.4.3 Radiation in snow and upper water body layers

The radiation properties of snow and water bodies are overwhelmingly determined by the complex spectral index of refraction, the snow density and particle structure, the surface structure (waves, roughness) and composition and by impurities in both bodies. Basics have been summarized in (82War) and (94Mob). The examples below should be considered to describe “typical” radiative transfer properties and can be used at least for first estimates in any investigation.

4.4.3.1 Snow

Snow can in a first approximation be considered to consist of small ice crystals of often complex shape between which many impurities are located due to sedimentation from the atmosphere. Also some algae can grow in the uppermost layers. Solar radiation can penetrate into snow to depths between about 20 to 40 cm. The stronger absorption at wavelength longer than about 0.45 µm causes a shift of the maximum spectral flux density towards the color blue. The total attenuation and also the scattering itself depend heavily on the structure and pureness of the snow layer. Thus a wide variety of attenuation characteristics can be found in the literature.

Snow becomes almost non-reflective at wavelengths larger than about 3 µm. Its emittance for thermal radiation is close to that of an ideal black body.

For easy use we publish in Fig. 4.4.3.1 some reflection curves from the measurements by Aoki et al. (00Aok) and from recent modeling work of the extinction in snow layers by King and Simpson. The spectral shape of the shown transmittance curves is overwhelmingly determined by the spectral properties of the index of refraction of ice. In some radiative transfer models different assumptions about the snow structure and shape of individual particles are made (e.g. 00Mae). We should add here, that pure and clean snow may reflect up to 90% of the incident solar radiation in the visible portion of the spectrum, whereas the reflectance becomes much smaller in the near infrared. Wet snow reflects usually much less than dry and fresh snow.

Figures 4.4.3.2 to 4.4.3.4 have been added for convenient extraction of reflection and extinction coefficients for diffuse radiation.

Table 4.4.3.1 summarizes a few measured albedo values of several stations.

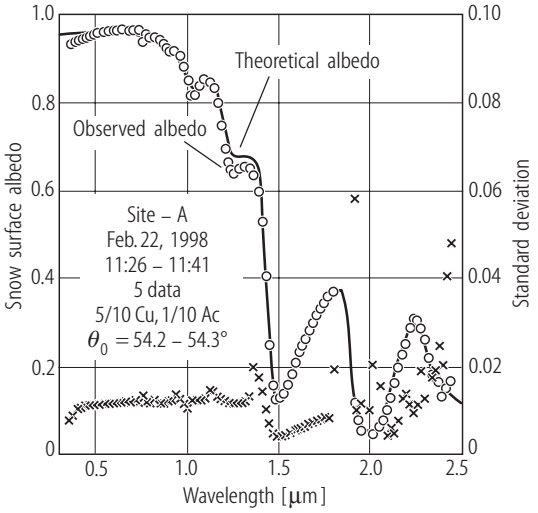

Fig. 4.4.3.1 Observed spectral albedo (left ordinate), the standard deviation (right ordinate) and theoretically calculated values for 4 models of the snow, which distinguish in the snow density and the concentration of impurities (from Aoki et al., 2000; (00Aok)). Note the rapid decrease with increasing wavelength beginning at about 1μm. In the near infrared snow becomes almost "black". The crosses are indicating the standard deviation of measurements at each wavelength interval.

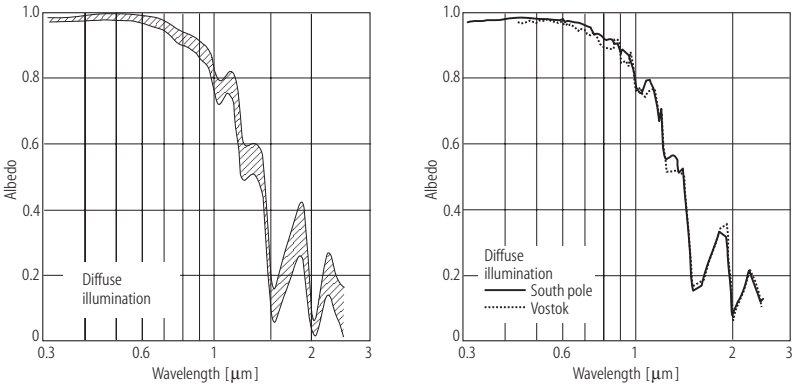

Fig. 4.4.3.2 Average spectral albedo of Antarctic snowfields for diffuse illumination, measured by Grenfell et al. 1994 (94Gre) at stations Vostok and South Pole.

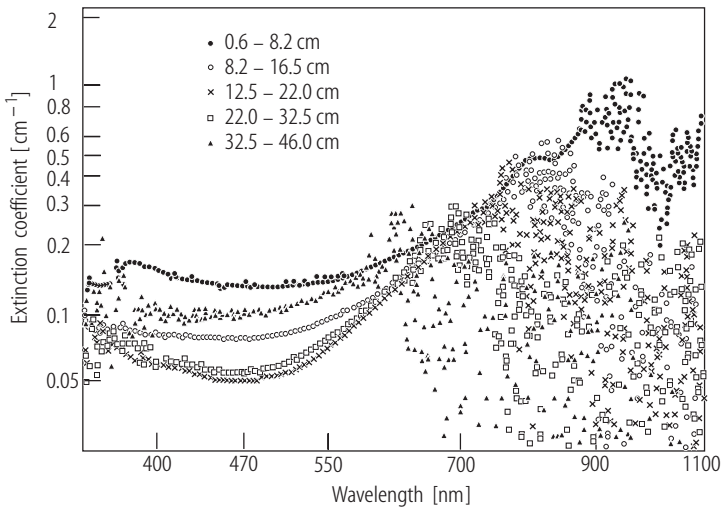

Fig. 4.4.3.3 Spectral extinction coefficients (in cm^{-1}) for diffuse solar radiation, derived from measurements of the downward solar radiation in alpine snow (02Bou). Note, the noise at larger wavelengths and depths is due to the weak signals as a consequence of the higher absorption in this spectral region. Approximate depths of measurement are given in the top left corner.

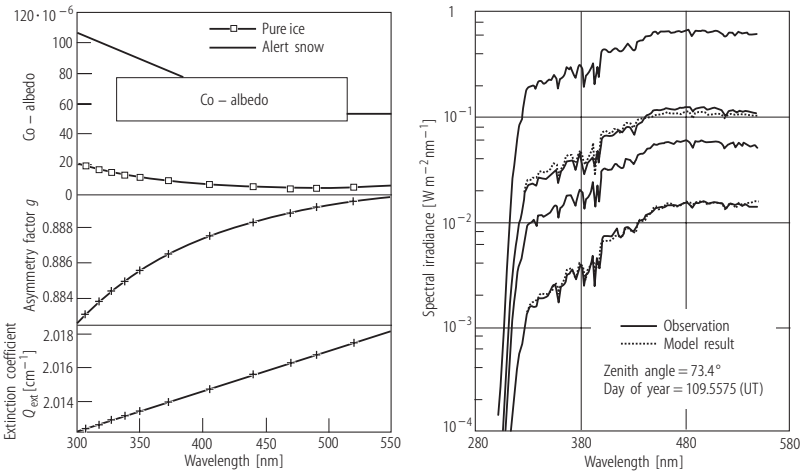

Fig. 4.4.3.4 Modeling of snow reflectance. Left: Optical properties of snow used in the model expressed by the co-albedo for single scattering, the asymmetry factor g and the extinction coefficient; right: measured and modeled downward spectral irradiances (from top downward) at the surface and at depths of 8.5, 12.6 and 20.4 cm (from 02Sim). These model results have been obtained in studies of photochemical processes in snow.

4.4.3.2 Radiative transfer properties of water bodies

The transfer of radiation in water bodies has been intensively studied for a variety of purposes. One of them is the remote observation of impurities in the oceans and rivers, which are important for estimates of the bioactivities and sediment transports in such aquatic systems. Another is the need for modeling of the upper ocean and lake heating by absorption of solar radiation in layers of up to about 50 cm thickness and the downward mixing of this heat. Terrestrial heat radiation is emitted from and absorbed within the uppermost layers of a few micrometers thickness, causing the so-called cold skin of the ocean, which can be up to 2 K colder than layers below.

The reflectance of a flat water surface for unidirectional incident radiation amounts in the visible part of the spectrum to about 0.03 and somewhat less in the near infrared, when the source is overhead. It increases with increasing zenith angle, as described by the basic Fresnel's law. In reality natural water surfaces are simultaneously illuminated by direct solar and diffuse solar radiation, where contribution of both components depends on the aerosol content and cloud cover of the sky and the Sun's zenith angle. Thus the effective albedo at clear sky may rise up to 5 to 7 percent in the visible and somewhat less in the near infrared. Further enhancements occur by waves of various wavelengths. Foam on the surface and particles within the near surface layers can easily be identified and even classified with multi-spectral measurements. But their contribution to the albedo for the solar radiation within the entire spectral range between about 0.4 and 1.5 μm is very small.

The curve below in Fig. 4.4.3.5 shows an earlier summary of measurements and can be used for practical estimates.

In all numerical simulations of radiative transfer in water bodies one needs to take into account the very strong forward scattering, which is due to both Hydrosols and density fluctuations in the water. A typical curve is shown below.

Table 4.4.3.1 Albedo for global radiation (total albedo) (monthly values, albedo-ranges given in brackets in the second lines are those with a snow cover)

Surfaces	Albedo values		Sources
	Observed range	Most frequent value	
Glacier, accumulation area	0.57 - 0.85	0.75	94Gre, 56Lil, 01Ohm
Glacier, equilibrium line area (in melt period)	0.37 - 0.77	0.65	96Cut, 01Ohm
Glacier, ablation area (after snow melt)	0.11 - 0.70	0.35	96Cut, 01Ohm, 02Tak
Bare rock	0.09 - 0.28	0.21	65Dav, 73Kon, 69Kon, 85Rot, 65Sel, 94Sie
Seasonal snow cover, clean (before melt period)	0.65 - 0.85	0.70	81Gre, 73Kon, 82Ohm, 01Ohm, 94Sie, 01Z'g
Seasonal snow cover, clean (during the melt)	0.3 - 0.6	0.4	- as above -
Dirty snow cover	0.2 - 0.4	0.3	73Kon, 82Ohm, 84Shu, 01Z'g
Tundra (in snow-free period)	0.07 - 0.22	0.15	82Ohm, GEBA
Natural boreal forest, close crown (Canada)	0.04 - 0.17	0.10	65Dav
Natural boreal forest, open woodland (Canada)	0.07 - 0.19	0.12	65Dav
Natural boreal forest, close crown (Siberia)	0.12 - 0.21	0.16	01Kob
Burned boreal forest, close crown (Siberia)	0.10 - 0.18	0.14	01Kob
Managed forest (Pinus) (Germany)	0.09 - 0.13 (0.15-0.25)	0.10	99Kes
Managed forest (Abies) (Switzerland)	0.05 - 0.06 (0.21-0.30)	0.06	94Sie
Bog and Muskeg	0.05 - 0.17	0.11	65Dav
Deciduous forest, before fall	0.10 - 0.20	0.15	78Lee, 85Rot, 94Sie
Deciduous forest, after fall	0.08 - 0.15	0.11	- as above -
Step	0.09 - 0.25	0.17	73Kon, 69Kon, GEBA
Dry step	0.22 - 0.26	0.25	73Kon, GEBA
Desert	0.24 - 0.28	0.25	73Kon, 65Sel, BSRN
Tall grass	0.22 - 0.33	0.27	73Kon, 65Sel, 98Tsay
Tropical forest	0.11 - 0.15	0.12	99Gia, 82Pin, 98Ros, 89Shu, 84Shu, 98Tsay
Agricultural field, bare soil	0.08 - 0.14	0.10	85Rot, 65Sel, 94Sie
Agricultural field, with plants	0.14 - 0.27 (0.24-0.73)	0.17	- as above - 70Ogu
Short grass (meteorol. stations)	0.21 - 0.25	0.22	73Kon, 85Rot, 94Sie
Cities	0.11 - 0.18 (0.18-0.37)	0.15	78Oke, 85Rot, 94Sie GEBA
Lakes	0.02 - 0.16	0.08	73Kon, 85Rot, 94Sie
Ocean (open water) (Albedo of water depends heavily on the incidence angle of radiation.)	0.03 - 0.45	0.08	72Pay, - as above -
Sea ice before melt (excl. leads)	0.75 - 0.88	0.83	01Ohm, 02Per, 02Pers
Sea ice during melt (excl. leads and ponds)	0.25 - 0.82	0.50 - 0.65 as above	
Melting white ice	0.55 - 0.72	0.65	02Per, 02Pers
Melting blue ice	0.25 - 0.32	0.28	- as above -
Ponds on sea ice	0.10 - 0.30	0.20	- as above -

4.5 A few final remarks

This section summarizes a most complete data set on the radiation budget components at the TOA and at ground, which have been computed within the International Cloud Climatology Project (ISCCP) from satellite-borne radiance measurements and in the radiation measurements at the ground-level Baseline Radiation Network (BSRN). Further a few other quantities are given describing the PAR and UV at ground. This data can be used in education and research. It provides a good basis for studies of the radiative heating of continental, snow and ice surfaces, and also of water bodies. A deeper scientific discussion is available in the current scientific literature of which we only quote a very small fraction. We also provided a few internet links, where further data and information can be obtained.

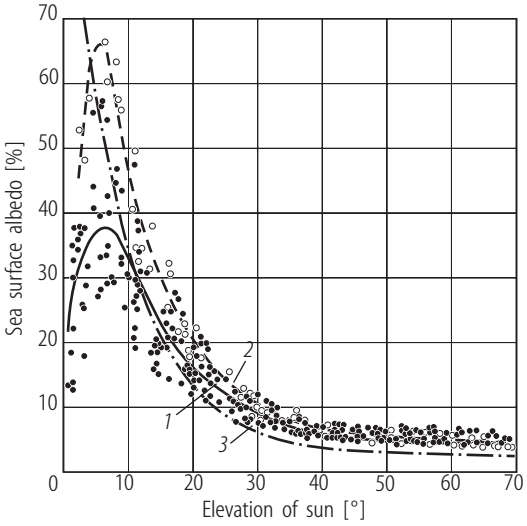

Fig. 4.4.3.5 Effective values of the sea surface albedo as derived from many ship-borne measurements (summarized by (73Kon)) plotted vs. the elevation h of the Sun. These curves are based on a synopsis of measurements made by many different groups and should also illustrate the ranges of uncertainties of such measurements from ship, buoys or aircraft over the sea. The final decrease of the reflectance towards very low **elevations h** of the Sun can be explained by enhanced absorption due to small wavelets on the ocean surface and by the relative dominance of scattered global radiation. These values must be understood to contain both components, the direct and diffuse downward solar radiation.

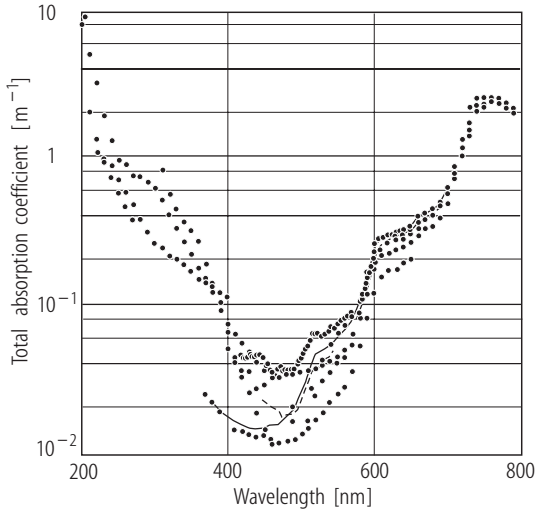

Fig. 4.4.3.7 Total absorption coefficient for **natural freshwater**, as given by various authors (from 81Smi). The large scattering of results in the area of the absorption minimum is due to impurities in the water probes. These curves are used in various remote sensing applications, whereby several additional absorbing and scattering materials are added in simulations.

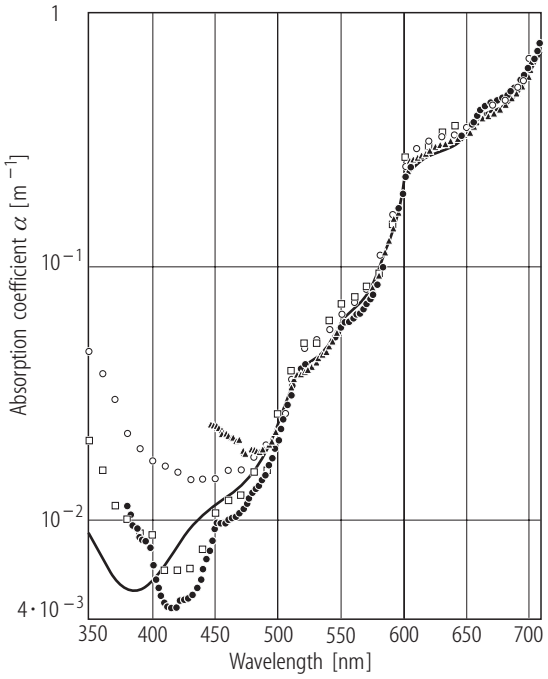

Fig. 4.4.3.6 Absorption of pure water, as obtained by various authors and summarized by (97Pop). This data can be used for simulating investigations with cleanest water probes in the laboratories.

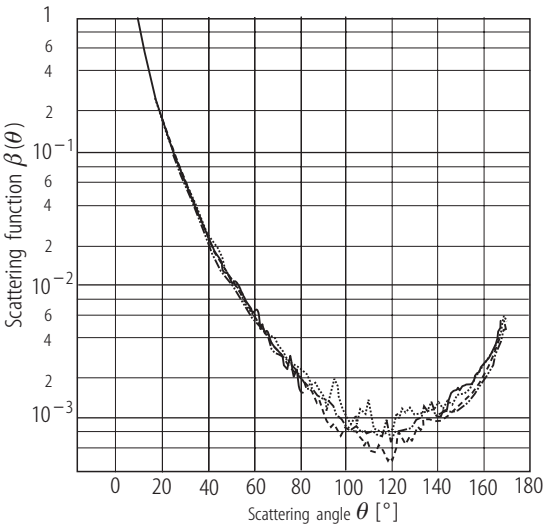

Fig. 4.4.3.8 Mean effective scattering functions of natural water probes at 440, 490, 550 and 670 nm, as measured at 15 m depth, normalized to the value 1 at 10° to remove changes in the magnitude (from Pegau et al., 1995; 95Peg). The strong forward peak enables in very clean water the penetration of blue light into layers as deep as 100 m. The abscissa describes the scattering angle, where forward scattering means 0°, and backward scattering 180°.

A still open major problem is the validation of such data. The radiation fluxes at TOA can in principle be compared with those obtained from simultaneous measurements of other meteorological satellites as shown above. Ground-based measurements of the downward fluxes of solar and atmospheric radiation are made with often excellently calibrated and maintained instruments of mostly national networks. However, data from only a few stations are readily available for further use. Therefore we recommend a special validation project whose details need still careful consideration.

The initial comparison between such measurements showed a mean bias for monthly averages of the downward solar radiation at ground of about 5 to 20 Wm^{-2} (possibly too high estimates from ISCCP data) and of an uncertainty of 10 to 20 Wm^{-2} for terrestrial radiation, respectively. This would explain the rather low cloud effect on the vertical divergence of solar radiation. Future work therefore must concentrate on validations of ground-based measurements and on the error analysis of the radiation climatology shown here.

At the end it should not be overlooked, that during the past about 10 years the analyses of satellite data with respect to their information content on important environmental parameters, such as the PAR and the associated biomass production (e.g. 03Ber) or the atmospheric ozone and the UV-B at ground (e.g. 00Gob), and in particular also on parameters of the radiation budget in the climate system have been developed further to stages where they now become more or less operational. In parallel various national an international ground-based networks have also been established. Only the combined use of space-borne and ground-based measurements in conjunction with careful calibrations will allow to monitor with high confidence regional and global changes of these climate characteristics. We refer here also the reader to the rich information in various websites to be found under headers like UV-B, or Photosynthetically Active Radiation, or Planetary Radiation Budget.

4.6 References for 4

56Lil Liljequist, G.H.: Energy exchange of an Antarctic snow-field, Part 1, Short-wave radiation (Maudheim, 71º 03' S, 10º 56' W), Norwegian-British-Swedish Antarctic Expedition 1949-1952: Scientific Results, Vol. 2 (1956). Oslo: Norsk Polar Institutt.

64Man Manabe, S., Strickler, R.F.: Thermal equilibrium of the atmosphere with a convective adjustment; J. Atmos. Sci. **21** (1964) 361-385.

65Dav Davies, J.A.: Albedo investigations in Labrador-Ungava. Archiv Meteorol. Geophys. Bioklimatol. Ser. B **13** (1965) 137-151.

65Sel Sellers, W.: Physical Climatology. Chicago: University of Chicago Press, 1965, 272 pp.

69Kon Kondratyev, K.Ya.: Radiation on the atmosphere. New York: Academic Press, 1969, 912 pp.

70Ogu Oguntoyinbo, J.S.: Reflection coefficients of natural vegetation, crops and urban surfaces in Nigeria; Q. J. R. Meteorol. Soc. **96** (1970) 430-441.

72Pay Payne, R.E.: Albedo of the sea surface. J. Atmos. Sci. **29** (1972) 959-970.

72Ras Raschke, E.: Die Strahlungsbilanz des Systems Erde-Atmosphäre - neuere Ergebnisse von Satellitenmessungen; Z. Geophys. **38** (1972) 967-1000.

73Kon Kondrat'ev, K.Ya.: Radiative characteristics of the atmosphere and the earth's surface. New Delhi: Amerind Publ., 1973, 580 pp.

74Kas Kasten, F., Raschke, E.: Reflection and transmission terminology by analogy with scattering; Appl. Opt. **13** (1974) 460-464.

78Lee Lee, R.: Forest Microclimatology (1978). New York: Columbia University Press, 1978, 276 pp.

78Oke Oke, T.R.: Boundary Layer Climates. London: Methuen, 1978, 372 pp.

81Gre Grenfell, T.C., Perovich, D.K., Ogren, J.A.: Spectral albedo of an alpine snow-pack; Cold Reg. Sci. Technol. **4** (1981) 121-127.

81Smi Smith, R.C., Baker, K.S.: Optical properties of the clearest natural waters (200 - 800 nm). Appl. Opt. **20** (1981) 177-184.

82Ohm Ohmura, A.: Climate and energy balance of an arctic tundra; J. Climatol. **2** (1982) 65-84.

82Pin Pinker, R.T.: The diurnal asymmetry in the albedo of tropical forest vegetation; Forest Science **28** (1982) 297-304.

82War Warren, S.G.: Optical properties of snow; Rev. Geophys. **20(1)** (1982) 67-89.

84Shu Shuttleworth, W.J., Gash, J.H., Lloyd, C.R., Moore, C.J., Roberts, J., Morgue, F., Nobre, J.C.A., Cabral, O.M.R., Patel, S.R., de Moares, J.C.: Observations of radiation exchange above and below Amazonian forest; Q. J. R Meteorol. Soc. **110** (1984) 1163-1169.

84War Warren, S.G.: Optical constants of ice from the ultraviolet to the microwave. Appl. Opt. **23** (1984) 1206-1225.

84Web Webster P.J., Stephens, G.L.: Cloud-radiation interaction and the climate problem. Chapt. 5 in John T. Houghton (ed.): The Global Climate (1984), Cambridge: Cambridge University Press 1984., pp 63-78.

85Rot Roth, M.: Albedomessungen über dem schweizerischen Mittelland. Diplomarbeit ETH Zürich, 1985, 114 pp.

86Sch Schanda, E.: Physical fundamentals of remote sensing. Springer Verlag, Heidelberg, 187 pp (1986).

89Shu Shuttleworth, W.J.: Micrometeorology of temperate and tropical forest. Philos. Trans. R. Soc.(London) B **324** (1989) 299-334.

90Har Harrison, E.F., Minnis, P., Barkstrom, B.R., Ramanathan, V., Cess, R.C., Gibson, G.G.: Seasonal variation of cloud radiative forcing derived from the earth radiation budget experiment; J. Geophys. Res. **95** (1990) 18687-18703.

92Cha Chahine, M.T.: The hydrological cycle and its influence on climate. Nature (London) **359** (1992) 373-380.

92Hus Husson, N., Bonnet, B., Scott, N.A., Chedin, A.: Management and study of spectroscopic information: the GEISA program; J. Quant. Spectrosc. Radiat. Transfer **48** (1992) 509-518.

92Lio Liou, K.: Radiation and cloud processes in the atmosphere. New York: Oxford Univ. Press. 1992, 487 pp.

92Pei Peixoto, J., Oort, A.: Physical Climatology, American Institute of Physics, 1992, 520 pp.

93And Anderson, G.P. Chetwynd, J.H., Theriault, J.-M., Archaya, P., Berk, A.R. Kneizys, F.X., Hoke, M.L., Abreu, L.W., Shettle, E.P.: MODTRAN 2: Suitability for remote sensing; Proc. Soc. Photo-Opt. Instrum. Eng. **168** (1993) 514-525.

93Hob Hobbs, P.V. (ed.): Aerosol-Cloud-Climate Interactions. San Diego: Academic Press, 1993, 233 pp.

93Tak Takeshita, S., Sudo, N., Sakata, T., Sasaki, M.: Daily, monthly and annual variations in the solar ultraviolet irradiance; Proc. Faculity of Engineering, Tokai University (English edition) **33(2)** (1993) 91-100.

94Gre Grenfell, T.C., Warren, S.G., Mullen, P.C.: Reflection of solar radiation by the Antarctic snow surface at ultraviolet, visible and near-infrared wavelengths; J. Geophys. Res. D **99(9)** (1994) 18669-18684.

94Har Hartmann, D.L.: Global Physical Climatology, San Diego: Academic Press, 1994, 411 pp.

94Mob Mobley, C.D.: Light and Water. San Diego: Academic Press, 1994, 592 pp.

94Sie Sie, R.: Die Albedo des Mittellandes. Diplomarbeit, ETH Zürich, Switzerland, 1994, 135 pp.

94Web Webster, P.J.: The role of hydrological processes in ocean-atmosphere interactions; Rev. Geophys. **32** (1994) 427-476.

95Fro Frouin, R., Pinker, R.: Estimation of Photosynthetically Active Radiation (PAR) at the earth's surface from satellite observations. Remote Sensing of Environ. **51** (1995) 98-107.

95Goo Goody, R., Yung, Y.L.: Atmospheric radiation. Theoretical basis. Oxford University Press, 1995, 536 pp.

95Peg Pegau, W.S., Zaneveld, R.V., Voss, K.J.: Towards closure of inherent optical properties of natural waters; J. Geophys. Res. C **100(7)** (1995) 13193-13199.

95Ros Rossow, W.B., Zhang, Y.-C.: Calculation of surface and top of the atmosphere radiative fluxes from physical quantities based on ISCCP data sets. 2. Validation and first results; J. Geophys. Res. D **100(1)** (1995) 1167-1197.

95Whi Whitlock, C.H., Charlock, T.P., Staylor, W.F., Pinker, R.T., Laszlo, I., Ohmura, A., Gilgen, H., Konzelmann, T., Di Pasqala, R.C., Moats, C.D., LeVroy, S.R., Ritchey, N.A.: The first ISCCP shortwave radiation budget data set; Bull. Am. Meteorol. Soc. **76** (1995) 905-922.

95Wie Wielicki, B.A., Cess, R.D., King, M.D., Randall, D.A., Harrison, E.F.: Mission to planet earth: Role of clouds and radiation in climate; Bull. Am. Meteorol. Soc. **76** (1995) 2125-2133.

95Zha Zhang, Y.-C., Rossow, W.B., Lacis, A.A.: Calculation of surface and top of the atmosphere radiative fluxes from physical quantities based on ISCCP data sets. 1. Method and sensitivity to input data uncertainties; J. Geoph. Res. D **100(1)** (1995) 1149-1165.

96Cut Cutler, P.M., Munro, S.: Visible and near-infrared reflectivity during the ablation period on Peyto Glacier, Alberta, Canada; J. Glaciol. **22** (1996) 333-340.

97Beh Behrenfeld, M.J., Falkowski, P.G.: A consumer's guide to phytoplankton primary productivity models; Limnol. Oceanogr. **42** (1997) 1479-1491.

97Bis Bishop, J.K.B., Rossow, W.B., Dutton, E.G.: Surface solar irradiance from ISCCP, 1983-1991; J. Geophys. Res. D **102** (1997) 6883-6910.

97Kie Kiehl, J., Trenberth, K.E.: Earth's annual global mean energy budget; Bull. Am. Meteorol. Soc. **78** (1997) 197-208.

97Ohm Ohmura, A.: New methods and findings concerning the total heat budget of the earth (in Japanese); Journ. Geograph. **106(954)** (1997). 762-763.

97Pop Pope, R.M., Fry, E.S.: Absorption spectrum (380 - 700 nm) of pure water. II. Integrating cavity measurements; Appl. Opt. **36** (1997) 8710-8723.

98Fro Froehlich, C., Lean, J.: The sun's total irradiance: Cycles, trends and related climate change uncertainties since 1976; Geophys. Res. Lett. **25** (1998) 4377-4380.

98Gil Gilgen, H., Wild, M., Ohmura, A.: Means and trends of shortwave irradiance at the surface estimated from global energy balance archive data; J. Clim. **11** (1998) 2042-2061.

98Mey Meywerk, J., Ramanathan, V.: Observations of the spectral clear-sky aerosol forcing over the tropical Indian Ocean; J. Geophys. Res. D **104(20)** (1998) 24359-24370.

98Ohm Ohmura, A. (24 co-authors): Baseline Surface Radiation Network (BSRN/WRMC), a new precision radiometry for climate research; Bull. Am. Meteorol. Soc. **79** (1998) 2115-2136.

98Ros Ross, J.L., Hobbs, P.V., Holben, B.: Radiative characteristics of the regional hazes dominated by smoke from biomass burning in Brazil: Closure tests and direct radiative forcing; J. Geophys. Res. D **103** (1998) 31925-31941.

98Rot Rothman, L., Rinsland, C.P., Goldman, A., Massie, S.T., Edwards, P.D., Flaud, J., Perrin, A., Camy-Peyret, C., Dana, V., Mandin, Y.-Y., Shroeder, J.W., Gamache, R.R., Wattson, R.B., Yoshino, K., Chance, K.V., Jucks, K.W., Brown, L.R., Nemtchinov, V., Varanasi, P.: The HITRAN Molecular Spectroscopic Database and HAWKS (HITRAN Atmospheric Workstation): 1996 Edition. J. Quant. Spectrosc. Radiat. Transfer **60** (1998) 665-710.

98Sei Seinfeld, J.H., Pandis, S.N.: Atmospheric chemistry and physics. (from air pollution to climate change). New York: John Wiley and Sons Inc., 1998, 1326 pp.

98Tsay Tsay, S., King, M.D., Arnold, G.T., Li, J.Y.: Airborne spectral measurements of surface anisotropy during SCAR-B; J. Geophys. Res. D **103** (1998) 31943-31953.

98Wil Wild, M., Ohmura, A., Gilgen, H., Roeckner, E., Giorgietta, M., Morcrette, J.-J.: The disposition of radiative energy in the global climate system: GCM-calculated versus observational estimates; Clim. Dyn. **14** (1998) 853-869.

99Gia Giambelluca, T.W., Fox, J., Yarnasarn, S., Onibutr, O, Nullet, M.A.: Dry-season radiation balance of land covers replacing forest in northern Thailand; Agri. For. Meteorol. **95** (1999) 53-65.

99Gil Gilgen, H., Ohmura, A.: The global energy balance archive; Bull. Am. Meteorol. Soc. **80** (1999) 831-850.

99Gre Grenfell, T., Warren, S.G.: Representation of a non-spherical ice particle by a collection of independent spheres for scattering and absorption of radiation; J. Geophys. Res. **104** (1999) 31697-31709.

99Jon Jones, P.D., New, M., Parker, D.E., Martin, S., Rigor, I.G.: Surface air temperature and its changes over the past 150 years; Rev. Geophys. **37** (1999) 173-198.

99Kes Kessler, A., Jaeger, L.: Long-term changes in net radiation and its components above a pine forest and a grass surface in Germany; Int. J. Clim. **19** (1999) 211-226.

99Pet Petit, J.R., Jouzel, J., Raynaud, D., 15 co-authors: Climate and atmospheric history of the past 420,000 years from the Vostok ice core, Antarctica; Nature (London) **399** (1999) 429-436.

99Qui Quinn, T.J., Froehlich, C.: Accurate radiometers should measure the output of the sun; Nature (London) **401** (1999) 801.

99Tho Thomas, G., Stamnes, K.: Radiative transfer in the atmosphere and ocean. Cambridge Univ. Press, Cambridge 1999, 510 pp.

00Aok Aoki, T., Aoki, T., Fukabori, M., Hachikubo, A., Tachibana, Y., Nishio, F.: Effects of snow physical parameters on spectral albedo and bi-directional reflectance of snow surface; J. Geophys. Res. D **105(8)** (2000) 10219-10236.

00Cro Crowley, T.J.: Causes of climate change over the past 1000 years; Science **289** (2000) 270-277.

00Froe Froehlich, C.: Observation of solar irradiance variability; Space Sci. Rev. **94** (2000) 15-24.

00Gob Gobron, N., Pinty, B., Verstraete, M.M., Widlowski, J.-L.: Advanced vegetation indices optimized for up-coming sensors: Design, performance and applications; IEEE Trans. Geosci. Remote Sensing **38(6)** (2000) 2489-2505.

00Lea Lean, J.: Evolution of the sun's spectral irradiance since the Maunder minimum; Geophys. Res. Lett. **27** (2000) 2425-2428.

00Mae Maetzler, Chr.: A simple snow pack/cloud reflection and transmittance model from microwaves to ultraviolet: the ice-lamella pack; J. Glaciol. **46** (2000) 20-24.

00Rei Reid, G.C.: Solar variability and the earth climate: Introduction and overview; Space Sci. Rev. **94** (2000) 1-11.

01Cho Choudhoury, B.J.: Estimating Gross photosynthesis using satellite and ancilliary data. Approach and preliminary data; Remote Sensing of Environ. **75** (2001) 1-21.

01Goe Goetsche, F.-M., Olesen, F.S.: Evolution of neural networks for radiative transfer calculations in the terrestrial infrared; Remote Sensing of Environ. **80** (2001) 157-164.

01IPC IPCC: Climate change 2001: The scientific basis. Cambridge University Press, Cambridge 2001, 881 pp.

01Kob Kobayashi, Y., Machimura, T., Iwahana, G., Fukuda, M., Fedorov, A. N.: Fire effect on flux and active layer dynamics in Taiga forest over Eastern Siberia permafrost region. In: Fukuda, M., Kobayashi, Y. (eds.): Research Report of Permafrost Disturbance and Induced Emission of Greenhouse Gases in 2002, Sapporo: Hokkaido University, 2001, 156-161.

01Lea Lean, J.: Solar irradiance and climate forcing in the near future; Geophys. Res. Lett. **28** (2001) 4119-4122.

01McK McKenzie, R.L., Seckmeyer, G., Bais, A.F., Kerr, J.B., Madronich, S.: Satellite retrievals of erythermal UV dose compared with ground-based measurements at northern and southern mid-latitudes; J. Geophys. Res. D **106** (2001) 24051-24062.

01Ohm Ohmura, A.: Physical basis for the temperature-based melt-index method; J. Appl. Meteorol. **40** (2001) 753-761.

01Z'g Z'graggen, L.: Strahlungsbilanz der Schweiz. Dissert., Nr. 14,158, ETH Zürich, 2001, 196 pp.

02Bou Bourgeois, S.: Extinction of solar radiation within snow cover. M.-Thesis, ETH Zuerich, Switzerland, 2002, 86 pp.

02Car Carslaw, K.S., Harrison, R.G., Kirkby, J.: Cosmic rays, clouds and climate; Science **298** (2002) 1732-1737.

02Per Perovich, D.K., Light, B., Hobbs, P.V.: Seasonal evolution of the albedo of multi year Arctic sea ice; J. Geophys. Res. C **107 C10** (2002) 8044, doi:10.1029/2000JC000438, 2002.

02Pers Persson, P.O.G., Fairall, C.W., Andreas, E.L., Guest, P.S., Perovich, D.K.: Measurements near the atmospheric surface flux group tower at SHEBA; J. Geophys. Res. C **197 C10** (2002) doi: 10.1029/2000JC000705, 2002.

02Sim Simpson, W.R., King, M.D., Beine, H.J., Honrath, R.E., Zhou, X.: Radiation transfer modeling of snow-pack photochemical processes during ALERT 2000; Atmos. Environ. **36** (2002) 2663-2670.

02Tak Takeuchi, N.: Surface albedo and characteristics of cryoconite (biogenic surface dust) on an Alaska glacier, Gulkana Glacier in the Alaska Range; Bull. Glacier Res. **19** (2002) 63-70.

02Wie Wielicki, B.A., Wong, T., Allan, R.P., Slingo, A., Kiehl, J.T., Soden, B.J., Gordon, C.T., Miller, A.J., Yang, S.-K., Randall, D.A., Robertson, F., Susskind, J., Jacobowitz, H.: Evidence for large decadal variability in the tropical mean radiative energy budget; Science **295** (2002) 841-844.

03Ber Bernhard, G., Booth, Ch.R., Ehramijan, J.C.: Real-time UV and column ozone from multi-channel UV radiometers deployed in he National Science Foundation's UV monitoring network. Proceedings of the SPIE 5156 (2003).

03Har Harrison, R.G., Carlslaw, K.S.: Ion-aerosol-cloud processes in the lower atmosphere; Rev. Geophys. **41** (2003) 3.

03Li Li, Z., Ackerman, T.P., Wiscombe, W., Stephens, G.L.: Have clouds darkened since 1995?; Science **302** (2003) 1150-1151.

03Mee Meerkötter, R., Verdebout, J., Bugliaro, L., Edvardsen, K., Hansen, G.: An evaluation of cloud effects on UV radiation from polar orbiting and geostationary satellites at high latitudes; Geoph. Res. Lett. **30(18)** (2003) 1956.

03Ros Rosenlof, K.H.: How water enters the stratosphere; Science **302** (2003) 1690-1691.

05Ras Raschke, E., Ohmura, A., Rossow, W.B., Carlson, B.E., Zhang, Y.-C., Stubenrauch, C., Kottek, M., Wild, M.: Cloud effects on the radiation budget based on ISCCP data (1991-1995). Int. J. Climatology – in print (2005)